US Army Corps of Engineers

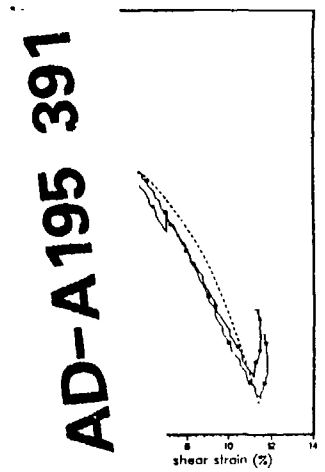

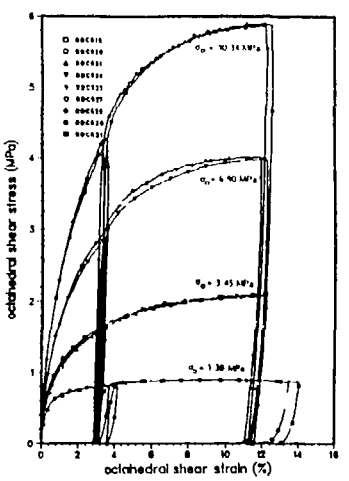

STRUCTURES LABORATORY

CONTRACT REPORT SL-88-3

AN ENDOCHRONIC PLASTICITY MODEL FOR ISST SOILS

by

K. C. Valanis

Endochronics, Inc.
Vancouver, Washington 98665

and

H. E. Read

S-CUBED, A Division of Maxwell Laboratories, Inc.
La Jolia, California 92038-1620

May 1988
Final Report

Prepared for DEPARTMENT OF THE ARMY
US Army Corps of Engineers
Washington, DC 20314-1000

Under Project No. 4A161102AT22, Task BO, Work Unit 005
(Contract No. DACA39-86-C-0030)

Monitored by Structures Laboratory
US Army Engineer Waterways Experiment Station
PO Box 631, Vicksburg, Mississippi 39180-0631

Destroy this report when no longer needed. Do not return it to the originator.

The findings in this report are not to be construed as an official Department of the Army position unless so designated by other authorized documents.

The contents of this report are not to be used for advertising, publication, or promotional purposes. Citation of trade names does not constitute an official endorsement or approval of the use of such commercial products.

Unclassified

SECURITY CLASSIFICATION OF THIS PAGE

REPORT DOCUMENTATION PAGE

Form Approved OMB No. 0704-0188 Exp. Date: Jun 30, 1986

1a. REPORT SECURITY CLASSIFICATION: Unclassified	1b. RESTRICTIVE MARKINGS
2a. SECURITY CLASSIFICATION AUTHORITY	3. DISTRIBUTION/AVAILABILITY OF REPORT: Approved for public release; distribution unlimited.
2b. DECLASSIFICATION/DOWNGRADING SCHEDULE	
4. PERFORMING ORGANIZATION REPORT NUMBER(S): SSS-R-88-9375	5. MONITORING ORGANIZATION REPORT NUMBER(S): Contract Report SL-88-3
6a. NAME OF PERFORMING ORGANIZATION: S-CUBED, A Division of Maxwell Laboratories, Inc. / 6b. OFFICE SYMBOL (If applicable)	7a. NAME OF MONITORING ORGANIZATION: USAEWES Structures Laboratory
6c. ADDRESS (City, State, and ZIP Code): PO Box 1620 La Jolla, CA 92038-1620	7b. ADDRESS (City, State, and ZIP Code): PO Box 631 Vicksburg, MS 39180-0631
8a. NAME OF FUNDING/SPONSORING ORGANIZATION: US Army Corps of Engineers / 8b. OFFICE SYMBOL (If applicable)	9. PROCUREMENT INSTRUMENT IDENTIFICATION NUMBER: DACA39-86-C-0030
8c. ADDRESS (City, State, and ZIP Code): 20 Massachusetts Avenue, NW Washington, DC 20314-1000	10. SOURCE OF FUNDING NUMBERS: PROGRAM ELEMENT NO. / PROJECT NO. 4A161102AT22 / TASK NO. BO / WORK UNIT ACCESSION NO. 005

11. TITLE (Include Security Classification): An Endochronic Plasticity Model for ISST Soils

12. PERSONAL AUTHOR(S): Valanis, K. C. and Read, H. E.

13a. TYPE OF REPORT	13b. TIME COVERED	14. DATE OF REPORT (Year, Month, Day)	15. PAGE COUNT
Final report	FROM Jul 86 TO Dec 87	May 1988	78

16. SUPPLEMENTARY NOTATION: Available from National Technical Information Service, 5285 Port Royal Road, Springfield, VA 22161.

17. COSATI CODES		
FIELD	GROUP	SUB-GROUP

18. SUBJECT TERMS (Continue on reverse if necessary and identify by block number)
Dilatancy; ~~ISST soil data~~; Endochronic soil models; Shear-induced volume change; Ground shock; Stress-strain relations.

19. ABSTRACT (Continue on reverse if necessary and identify by block number)

A new endochronic plasticity model that has the capability to describe both densification and dilatancy is described and applied to laboratory data from reconstructed ISST soils generated by the US Army Engineer Waterways Experiment Station. An efficient, explicit numerical scheme is developed for integrating the system of equations which govern the new model, and a corresponding computer program for the numerical scheme is given. In numerical studies conducted with the computer program, it was found that situations arise where the calculated intrinsic time increment takes on inadmissable values; this difficulty does not appear to be of numerical origin but instead due to the particular mathematical representations adopted in the model for some of the material functions. Further study is recommended to explore this problem. Keywords: Endochronic plasticity; Hydrostatic compression tests; Triaxial soil tests

20. DISTRIBUTION/AVAILABILITY OF ABSTRACT	21. ABSTRACT SECURITY CLASSIFICATION
☒ UNCLASSIFIED/UNLIMITED ☐ SAME AS RPT. ☐ DTIC USERS	Unclassified
22a. NAME OF RESPONSIBLE INDIVIDUAL	22b. TELEPHONE (Include Area Code) / 22c. OFFICE SYMBOL

DD FORM 1473, 84 MAR — 83 APR edition may be used until exhausted. All other editions are obsolete.

SECURITY CLASSIFICATION OF THIS PAGE

Unclassified

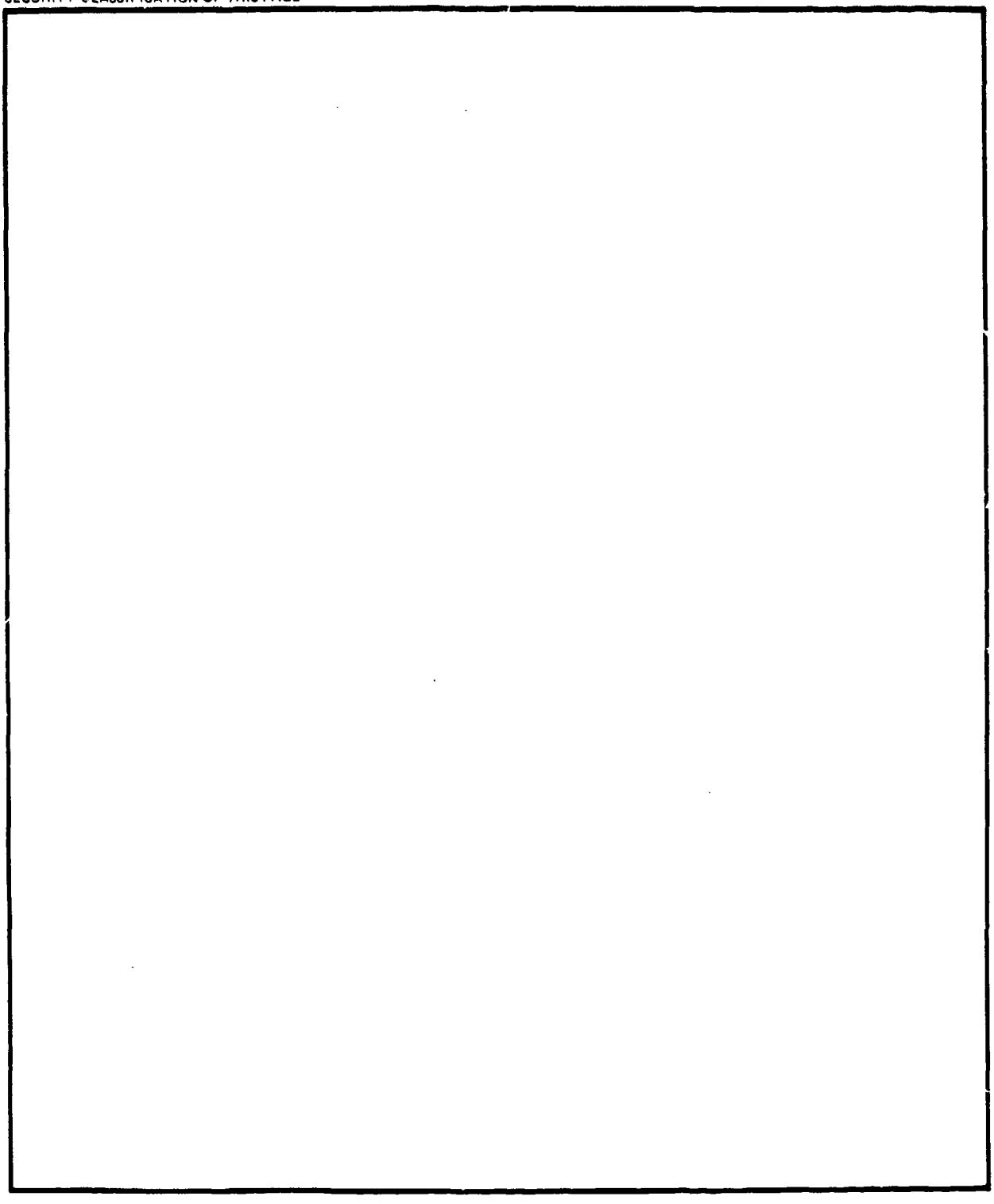

PREFACE

The research reported herein was performed by S-CUBED, a division of Maxwell Laboratories, Inc., and its subcontractor, Endochronics, Inc., during the period July 1986 through December 1987 for the US Army Engineer Waterways Experiment Station (WES) under Contract No. DACA39-86-C-0030. It was sponsored by the Office, Chief of Engineers, US Army, as a part of Project 4A161102AT22, Task BO, Work Unit 005, "Constitutive Properties for Natural Earth and Manmade Materials."

The co-principal investigators for the project and authors of this report were Dr. H. E. Read of S-CUBED and Dr. K. C. Valanis of Endochronics, Inc. The authors express their sincere appreciation to Mr. R. G. Herrmann, also associated with S-CUBED, who provided excellent computational support through the course of the research. The work was technically supported and monitored by Dr. G. Y. Baladi of the Geomechanics Division, Structures Laboratory (SL), WES. Dr. J. G. Jackson, Jr., was the WES Contracting Officer's Representative. Mr. Bryant Mather was Chief, SL.

COL Dwayne G. Lee, CE, is Commander and Director of WES. Dr. Robert W. Whalin is WES Technical Director.

Table of Contents

Table of Contents (concluded)

List of Illustrations

List of Illustrations (concluded)

Section 1

INTRODUCTION

In July 1986, a research program was initiated by S-CUBED and its subcontractor, ENDOCHRONICS, INC., for the purpose of developing an advanced constitutive model of ISST soils based upon the concepts of endochronic plasticity.[1-3] The research was sponsored by the U.S. Army Engineer, Waterways Experiment Station (WES) as part of its continuing effort to pursue the development and validation of new and improved analytical methods for predicting explosively-induced ground motion. In order to have a complete and reproducible set of ISST data appropriate for this purpose, WES performed a series of laboratory tests on reconstituted ISST soil samples.[4] Some of the tests in this series were of a special nature, such as shearing at constant hydrostatic pressure, to provide the type of data that are most convenient for fitting the endochronic model.

The model development was conducted in two phases, for reasons that will become apparent in the sequel. In the first phase, which was initiated in July 1986, the then existing version of the endochronic model (see Ref. 5, for example) was applied to the ISST data provided by WES. It was realized at the time that this endochronic model was only capable of predicting compaction during shearing at constant hydrostatic pressure. Thus, dilatancy cannot be described by this model. A cursory review of data from other sandy soils similar to the ISST soil conducted prior to the program had indicated that this limitation of the model would probably not be serious. The issue turned out to be much more complex than we expected, however, for reasons to be discussed in the text.

Prior to applying the model to the WES data, the data were processed on the basis of the usual recommendations of WES, as described in Ref. 6, that is, volumetric strains for cases of pure hydrostatic compression were defined on the basis of the "uniform" approximation, while volumetric strains generated during a process where shear was involved were defined according to the "cone" approximation. It was found that, when data involving shear are processed on the basis of the "uniform" approximation, dilatancy is usually observed while, if the "cone" approximation is used to process the data, compaction will be predicted. Thus, there is the potential for serious inconsistencies between predictions and data, which were vividly confirmed in the first phase of this study.

The inconsistency arises due to the fact that the purely hydrostatic component of a model is usually fit to data which has been processed on the basis of the uniform approximation. This component is then used as part of the more general model to predict the volumetric component of response in cases of non-isotropic loading, involving shear. In such cases, the predicted volumetric response will be the result of a model based on the uniform approximation, while the data, processed in the recommended fashion, would be based on the "cone" approximation. Because of this, the model will most likely predict dilatancy while the data will probably show compaction. The results obtained from the first phase of this study in which the endochronic model was fit to the ISST data in the recommended manner dramatically confirmed these inconsistencies.

Unfortunately, there appears to be no precise way of accurately defining the volumetric strain, needed for constitutive model development, from the usual triaxial data. The difficulty arises from the fact that the strain fields in triaxial tests are typically inhomogeneous. In view of this, and given that the usual data from the triaxial test gives the nominal engineering axial strain ϵ_a over the specimen length and the nominal engineering radial strain ϵ_r at the midpoint of the specimen, it appears that, while admittedly nor rigorous, the simple expression

$$\epsilon = \epsilon_a + 2\epsilon_r \qquad (1)$$

appears to provide the best definition of the nominal engineering volumetric strain that is possible within the limitations of the data provided. Several techniques for more accurately measuring strain in triaxial tests have recently been proposed (see Refs. 7 and 8, for example). Until such techniques have been implemented, however, Eq. (1) appears to be the preferred way of defining volumetric strain from triaxial data.

In view of the difficulties encountered in the first phase of the study due to the use of the uniform and cone approximations, it was mutually agreed by WES and S-CUBED that a second phase should be undertaken, using data that are processed only on the basis of Eq. (1), which to first order is the uniform approximation. This eliminates the inconsistencies that can arise from the joint

use of the "cone" and "uniform" approximations. However, another problem develops, since the use of Eq. (1) in conjunction with the ISST data will lead to dilatancy, which is not within the scope of the endochronic model used in the first phase. Therefore, an endochronic model with the capability to describe dilatancy is needed. Fortunately, such a model had very recently become available,[9,10] but had not been validated or applied to real materials.

The second phase of this study, which began in April 1987, was undertaken for the purpose of exploring the application of the new dilatant endochronic model[9,10] to the ISST soil data, using Eq. (1) to define volumetric strain from the data. The present report has been prepared mainly to summarize this work. In Section 2, the new dilatant endochronic model is described and the special case of shear at constant pressure is considered. The application of the model to the ISST data is described in Section 3. A numerical scheme and corresponding computer program for computationally dealing with the model are described in Section 4. Also, in this section, the case of shear at constant pressure is considered numerically. Section 5 discusses some difficulties that were encountered in the numerical study, and suggests possible ways to solve them. Finally, the conclusions drawn from this study, as well as recommendations for further study, are given in Section 6.

Section 2

AN ENDOCHRONIC SOIL MODEL WITH DILATANCY

2.1 BASIC CONSIDERATIONS.

The application of endochronic plasticity to soils has, so far, been limited either to one-dimensional histories (shear and hydrostatic response) under cyclic and other loading-unloading conditions or to two-dimensional histories (shear-volume interaction) under densifying conditions. The question of dilatant behavior has hitherto remained unresolved, in the sense that, until now, the constitutive relation in question [11] gave rise to densification in the presence of shearing under constant hydrostatic stress.

What is needed is a constitutive equation which under conditions of low density and/or high pressure will give rise to shear-induced densification but under conditions of high density and/or low pressure will give rise to shear-induced dilatancy. In this section we present a thermodynamic approach which leads to such characteristics of soil behavior. The full analysis is given in detail in Ref. 10.

The reasoning that led to the present treatment is broadly as follows. The coupling between deviatoric and hydrostatic behavior, that ultimately leads to dilatant deformation, must come from three possible sources:

(i) The intrinsic time through the shear-volumetric coupling parameter k;
(ii) The expression for the free energy;
(iii) The rate equations for the internal variables.

Source (i) alone, will always give rise to densification, as the application of the relevant equations actually showed. Source (ii) is not physically viable because given a soil with a certain porosity the onset of dilatancy under monotonic shearing is governed by the prevailing hydrostatic stress. If (ii) is to be the source, then a change in the form of the free energy must take place upon varying the hydrostatic stress, a phenomenon which does not appear physically plausible. One would expect the form of the free energy to remain invariant with a change in the hydrostatic stress. The remaining plausible cause is source (iii) and this is the one that we developed in Ref. 10 and summarize in the present work.

2.2 FORMULATION OF MODEL.

In Ref. 10 we took the position that whereas the deviatoric plastic work is a cause of hydrostatic plastic strain, it is external to the hydrostatic process in the sense that it is not a hydrostatic mechanism. Therefore, it qualifies as a thermodynamic internal force of the first kind in the sense of Ref. 12. In the presence of such forces the thermodynamic equations appropriate to the rigid plastic solid that represents the plastic behavior of the soil are the following, in the usual notation, in terms the deviatoric and hydrostatic free energies ψ_D and ψ_H respectively. For a more detailed thermodynamic treatment see Ref. 13.

$$\psi_D = \frac{1}{2} \sum A_r \left|\left| \underset{\sim}{e}^p - \underset{\sim}{q}_r \right|\right|^2 \tag{2}$$

$$\psi_H = \frac{1}{2} \sum B_r \left| \epsilon^p - q_r \right|^2 \tag{3}$$

$$\underset{\sim}{s} = \frac{\partial \psi_D}{\partial \underset{\sim}{e}^p} \quad , \quad \sigma = \frac{\partial \psi_H}{\partial \epsilon^p} \tag{4a,b}$$

$$\frac{\partial \psi_D}{\partial \underset{\sim}{q}_r} + a^r_{11} \frac{d\underset{\sim}{q}^r}{dz} = 0 \tag{5}$$

$$\frac{\partial \psi_H}{\partial q_r} + a^r_{22} \frac{dq_r}{dz} = R_r \tag{6}$$

where

$$R_r = - a^r_{21} \underset{\sim}{s} \cdot \frac{d\underset{\sim}{e}^p}{dz} \qquad \left(a^r_{21} > 0\right) \tag{7}$$

Thus R_r is a thermodynamic force of the first kind, i.e., one which is internally applied but which is external to the (internal) mechanism on which it operates.[12] The role of the coefficient a^r_{21} is to determine the degree to which the plastic work affects the r'th hydrostatic mechanism.

The intrinsic time dz is given by the customary relation

$$dz^2 = \left|\left|d\underset{\sim}{\epsilon}^p\right|\right|^2 + k^2|d\epsilon^p|^2 \qquad (8)$$

The resistance coefficients a^r_{11} and a^r_{22} are not constant but are related to the hardening functions F_D and F_H respectively by the equations

$$a^r_{11} = F_D\, a^{ro}_{11} \quad , \quad a^r_{22} = a^{ro}_{22}\, F_H \qquad (9a,b)$$

where

$$F_D = F_D(\sigma, z) \quad , \quad F_H = F_H(\epsilon^p) \qquad (10a,b)$$

The dependence of F_D on z is weak so that for deformations other than cyclic, for which the variation in z is small, the latter plays a minor role in F_D and may be ignored. The question as to whether the dilatancy coefficients a^r_{21} are constant during the deformation, or whether they change with hardening, is an open one at the moment. In this work they have been taken as constant and this choice seems to be consistent with experiment.

A straightforward analysis using Eqs. (2) to (7) in light of the initial conditions

$$\underset{\sim}{q}_r(0) = \underset{\sim}{0}, \quad q_r(0) = 0 \qquad (11a,b)$$

gives rise to the following set of two constitutive equations that govern, respectively, the deviatoric and hydrostatic behavior of soils:

$$\underline{s} = \int_0^{z_D} \rho(z_D - z') \frac{d\underline{e}^p}{dz'} dz' \tag{12}$$

$$\sigma = \int_0^{z_H} \phi(z_H - z') \frac{d\epsilon^p}{dz'} dz' + \int_0^{z_H} \Gamma(z_H - z') \underline{s} \cdot \frac{d\underline{e}^p}{dz'} dz' , \tag{13}$$

where the kernels ρ, ϕ and Γ are all weakly singular but integrable in any finite domain [0,z] and:

$$dz_D = \frac{dz}{F_D} , \quad dz_H = \frac{dz}{kF_H} \tag{14a,b}$$

$$\rho = \sum_r A_r \, e^{-\alpha_r z_D} \tag{15}$$

$$\phi = \sum_r B_r \, e^{-\beta_r z_H} \tag{16}$$

$$\Gamma = \sum_r \beta_r \frac{a_{21}^r}{F_H} e^{-\beta_r z_H} \tag{17}$$

$$\alpha_r = \frac{A_r}{a_{11}^{ro}} , \quad \beta_r = \frac{B_r}{a_{22}^{ro}} \tag{18a,b}$$

Some simplifications occur when the effect of the deviatoric plastic work rate is distributed uniformly among the hydrostatic mechanisms, in which case

$$a_{21}^{ro} = a_{21}^{o} \quad \text{(for all r)} \tag{19}$$

In this event, and in view of Equations (16) and (17)

$$\Gamma(z_H) = a_{21}^{o}\, \phi(z_H) \tag{20}$$

so that once $\phi(z_H)$ is known, from a simple monotonic hydrostatic test, then $\Gamma(z_H)$ is also determined within a multiplicative constant.

In addition there exist the elastic relations

$$d\underset{\sim}{e}^{e} = d\underset{\sim}{s}/2G \quad ; \quad d\epsilon^{e} = d\sigma/K \tag{21}$$

where μ is the elastic shear modulus, and K the elastic bulk modulus neither of which need be constant in the course of deformation. The total strain is given by the relations:

$$d\underset{\sim}{e} = d\underset{\sim}{e}^{e} + d\underset{\sim}{e}^{p} \quad ; \quad d\epsilon = d\epsilon^{e} + d\epsilon^{p} \tag{22}$$

The general method for determining the form of the functions ρ, ϕ and Γ, the functions F_H and F_D, the elastic moduli G and K as well as the parameter k, from appropriate experiments, is a subject that will be discussed later on in this section. The specific determination of these functions and parameters for the WES ISST soil is addressed in Section 3.

2.3 GENERAL APPROACH FOR DETERMINING MATERIAL FUNCTIONS AND PARAMETERS.

In this section, the general approach for determining the material functions and parameters of the endochronic model described in the preceding section is given. The functions and parameters that need to be determined for a particular material are: K, G, k, $\rho(z_D)$, $\phi(z_H)$, F_H and F_D.

The bulk modulus K, hydrostatic kernel $\phi(z_H)$ and the hardening function F_H can be determined from a pure hydrostatic test, which should have at least two unloadings and reloadings and extend well into the concave part of the virgin hydrostatic stress-strain curve. The data should consist of continuous measurements of σ and ϵ.

The shear modulus G, coupling parameter k, dilatancy parameter Γ_o, hardening function F_D and the shear kernel $\rho(z_D)$ are most efficiently determined from triaxial tests in which specimens are sheared under fixed hydrostatic (not confining) pressure. The fixed hydrostatic pressures selected for these tests should adequately cover the hydrostatic range of interest; they should be reached monotonically and lie on the concave part of the virgin hydrostatic curve. The shearing should be taken out to where the shear stress has essentially reached a limiting value. The data should consist of continuous measurement of σ, ϵ, $\underset{\sim}{s}$ and $\underset{\sim}{e}$.

Specific details of the approach for determining the material functions and parameters from the types of data discussed above are given below.

2.3.1 The Bulk Modulus K.

The bulk modulus K at the onset of hydrostatic deformation is determined by the slope of the hydrostatic stress-strain curve at the origin. We denote this value of K by K_o. However, in the case of ISST soils it was found that K does not remain constant but varies with compaction. Simultaneously it becomes dependent on the elastic hydrostatic strain. This complex behavior is inferred by making the following observations:

(a) Upon loading to some value of σ and unloading to zero stress and reloading one finds that K (i.e., the slope of the hydrostatic stress-strain curve at the onset of reloading) is not equal to K_o.

(b) The reloading stress-strain curve almost retraces the unloading curve with the implication that unloading is virtually elastic, and because it is non-linear, obviously dependent on the elastic strain. This also implies that

plastic unloading in the stress-plastic strain space is almost vertical with the inference that $\phi(z_H)$ is close to a delta function. In mathematical terms K admits the representation:

$$K = K(\epsilon^e, \epsilon^p) \tag{23}$$

In ISST soils Eq. (23) is closely approximated by the multiplicative form given in Eq. (24), i.e.,

$$K = K_0(\epsilon^p) K_1(\epsilon^e) \tag{24}$$

where, without loss of generality, we may set $K_1(0) = 1$.

Now let P be a point on the hydrostatic strain axis, reached upon unloading from a value of σ. Then K_0 is determined from the initial slope of the reloading hydrostatic stress-strain curve at P (where $\epsilon^e = 0$) and K_1 from the shape of the unloading part of the hydrostatic curve, terminating at P.

2.3.2 The Hardening Function F_H.

At this point certain observations are in order. The hydrostatic response under purely hydrostatic conditions is given by Eq. (25), obtained by setting s equal to zero in Eq. (13). Thus

$$\sigma = \int_0^{z_H} \phi(z_H - z') \frac{d\epsilon^p}{dz'} dz' \tag{25}$$

Thermodynamic considerations support the position that ϕ is integrable, bounded and convex for all finite z_H. Thus

$$\int_0^{z_H} \phi(z')dz' < \infty \qquad \text{(for all finite } z_H\text{)} \tag{26}$$

If F_H were constant and equal to unity, say, then in view of Eqs. (25) and (26), z_H would be equal to ϵ^p and Eq. (25) would give σ as a convex function of ϵ^p. However in actual experiments σ becomes asymptotically a very rapidly increasing concave function of ϵ^p as ϵ^p increases. In particular this function is invariably of an exponential type, so that

$$\sigma = \phi_o \exp(\beta \epsilon^p) \tag{27}$$

for large values of ϵ^p. Equation (27) is a basic hypothesis of the critical state theory. If $\phi(z_H)$ were a delta function in the sense of Eq. (28), then,

$$\phi(z_H) = \phi_o \, \delta(z_H) \tag{28}$$

Thus in view of Eqs. (25), (8) and (14b):

$$\sigma = \phi_o \frac{d\epsilon^p}{dz_H} = \phi_o \, F_H \tag{29}$$

Comparison of Eqs. (27) and (29) yields the important result,

$$F_H = \exp(\beta \epsilon^p) \tag{30}$$

Consider now the other simple case where the hydrostatic response is given in terms of one internal variable. In this event the resulting constitutive response is given by the following equation:

$$\beta^* \sigma + (d\sigma/dz_H)^{\bullet} = \beta^* \phi_o (d\epsilon^p/dz_H) \quad , \tag{31}$$

which under monotonic loading conditions becomes the nonlinear differential equation:

$$\beta^* \sigma + (d\sigma/d\epsilon^p) F_H = \beta^* \phi_o F_H \,, \tag{32}$$

where β^* and ϕ_o are material constants.

We now ask the question as to what should the form of the hardening function be if the hydrostatic response is to be given, albeit asymptotically by Eq. (27). A simple substitution for σ (as given by Eq. (27)) in Eq. (31) gives rise to the following result:

$$F_H = \exp(\beta\epsilon^p) / \{1 - a \exp(\beta\epsilon^p)\} \tag{33}$$

where $a = \beta/\beta^*$. Now F_H is more complicated but still looks a great deal like an exponential function for small values of "a". It is of interest to note that in view of Eq. (32) it follows that as $\beta^* \to \infty$, $\phi(z_H)$ tends to a delta function, σ is given by Eq. (29) and F_H by Eq. (30), which is the limit of Eq. (33) as $a \to 0$.

2.3.3 The Kernel Function $\phi(z_H)$.

The function $\phi(z_H)$ can be determined uniquely from Eq. (25) if the form of the hardening function F_H is known *a priori*. To that end we note that there is sufficient experimental evidence to support the position the F_H is of exponential character and is given by Eq. (30). Under conditions of monotonic loading Eq. (25) then becomes:

$$\sigma(z_H) = \int_0^{z_H} \phi(z_H - z') F_H(z') dz' \tag{34}$$

where

$$\sigma(z_H) = \sigma\{\epsilon^p(z_H)\} \;; \quad F_H(z_H) = F_H\{\epsilon^p(z_H)\} \tag{35a,b}$$

In the case where Eq. (30) applies a simple calculation shows that

$$F_H = 1/(1 - \beta z_H) \tag{36}$$

Since now both σ and F_H are known, Eq. (34), which is a Volterra integral equation, may be solved numerically to give the unknown function $\phi(z_H)$.

In the actual case of ISST soil, the steepness of the unloading hydrostatic stress-strain curve indicated that $\phi(z_H)$ is indeed close to a delta function. In this event the numerical values of ϕ are so dominant near $z_H = z'$ that, by virtue of the mean value theorem, one can represent the integral on the right-hand side of Eq. (34) by the expression:

$$\sigma = F_H \int_0^{z_H} \phi(z_H - z')dz' = F_H \int_0^{z_H} \phi(z')dz' \tag{37}$$

Thus, in view of Eqs. (35) and (36):

$$\phi(z_H) = (d/dz_H)\{\sigma(z_H)(1 - \beta z_H)\} \tag{38}$$

2.3.4 The Material Constants k and Γ_o.

We begin with the hydrostatic constitutive equation, previously Eq. (13), which in the case of the cylindrical triaxial test becomes:

$$\sigma = \int_0^{z_H} \phi(z_H - z')\frac{d\epsilon^p}{dz'}\,dz' + \int_0^{z_H} \Gamma(z_H - z')\, s \bullet \frac{de^p}{dz'}\,dz' \tag{39}$$

where $s = \sqrt{2/3}(\sigma_2 - \sigma_1)$ and $e^p = \sqrt{2/3}(\epsilon_2^p - \epsilon_1^p)$, with x_1 being the axial direction.

The shear modulus G is presumed known. Its determination will be discussed later in the section. Thus e^p may be calculated from e via Eqs. (21) and (22).

Previously ϕ and Γ were represented by delta functions in the specific case where initial hydrostatic stress lay on the concave part of the hydrostat. Here we consider the more general case where ϕ and Γ are represented by an exponential function. Thus we set

$$\phi = \beta^* \phi_0 e^{-\beta^* z_H} \quad , \quad \Gamma = \beta^* \Gamma_0 e^{-\beta^* z_H} \tag{40}$$

Note that, in the limit as $\beta^* \to \infty$, the right-hand sides of Eqs. (40a,b) become delta functions, thereby recovering the previous case.

Using Laplace transforms one may now solve Eq. (39) in the light of Eqs. (41) and obtain the following expression for ϵ^p:

$$\epsilon^p = \frac{1}{\phi_0}\left[\frac{\sigma}{\beta^*} + \int_0^{z_H} \sigma dz'\right] - \frac{\Gamma_0}{\phi_0}\int_0^{z_H}\left(\underline{s} \cdot \frac{d\underline{e}^p}{dz'}\right)dz' \tag{41}$$

Now let $\sigma = \sigma_0$, where σ_0 is the constant hydrostatic stress at which shearing occurs, and let $d\epsilon_0^p$ be the increment in volumetric strain due to shear, at constant hydrostatic stress. Then differentiating Eq. (41) we obtain the following relation for $d\epsilon_0^p$:

$$\phi_0\left(\frac{d\epsilon_0^p}{dz_H}\right) = \sigma_0 - \Gamma_0\left(\underline{s} \cdot \frac{d\underline{e}^p}{dz}\right) \tag{42}$$

Note that the same equations would have been obtained had we represented ϕ and Γ by δ-functions. However, now there is an important difference in that σ_o is no longer equal to $e^{\beta\epsilon_o^p}$ where ϵ_o^p is the volumetric strain at the end of the (initial) hydrostatic phase. In fact, in the present case:

$$\sigma = \int_0^{z_H} \beta^* \phi_0 e^{-\beta^*(z_H - z')} e^{\beta\epsilon} dz' \tag{43}$$

or

$$\beta^*\sigma + \frac{d\sigma}{dz_H} = \beta^*\phi_0 e^{\beta\epsilon^p} \tag{44}$$

The effect is illustrated in Figure 1. Note that at low stresses the form $\phi = \phi_0\delta(z_H)$ seriously overestimates the initial hydrostatic stress.

Let us now recall Eqs. (8) and (42) with the constraint $\sigma = \sigma_o$, i.e.,

$$dz^2 = ||d\underline{e}^p||^2 + k^2(d\epsilon^p)^2 \tag{45}$$

$$\sigma_o dz = \phi_0 e^{\beta\epsilon} k d\epsilon^p + \Gamma_o \underline{s} \cdot d\underline{e}^p \tag{46}$$

except that now $\sigma_o \neq e^{\beta\epsilon}$ but is given by Eq. (43). Specifically in the case of the triaxial test:

$$dz^2 = (de^p)^2 + k^2(d\epsilon^p)^2 \tag{47}$$

$$\sigma_o dz = \phi_0 e^{\beta\epsilon^p} k d\epsilon^p + \Gamma_o s\, de^p \tag{48}$$

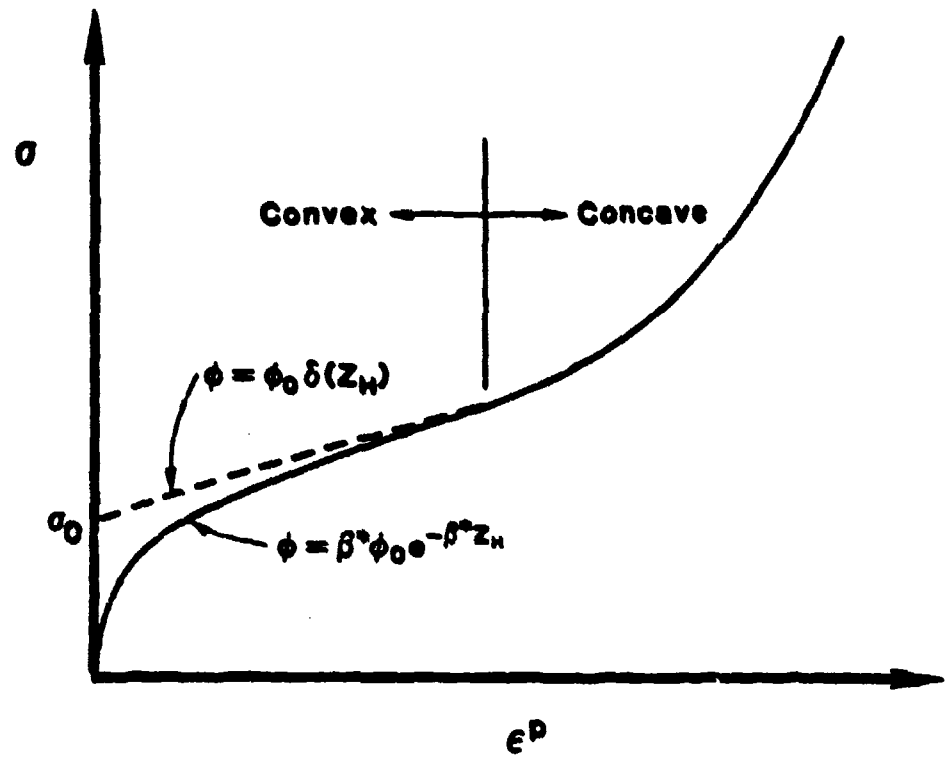

Figure 1. **Mean stress σ versus plastic volumetric strain ϵ^p.**

$$\text{where } s = \sqrt{\frac{3}{2}}\,(\sigma_1 - \sigma_2) \text{ and } e^p = \sqrt{\frac{3}{2}}\,(\epsilon_1^p - \epsilon_2^p) \qquad (48')$$

Equations (47) and (48) can be solved simultaneously to give:

$$k\,\frac{d\epsilon^p}{de^p} = \frac{1 - \left(\Gamma_o \frac{s}{\sigma_o}\right)^2}{\Gamma_o\left(\frac{s}{\sigma_o}\right)\frac{\phi_o}{\sigma_o}\,e^{\beta\epsilon^p} + \left[\frac{e^{2\beta\epsilon^p}}{\sigma_o^2}\,\phi_o^2 + \left(\frac{s}{\sigma_o}\right)^2\Gamma_o^2 - 1\right]^{1/2}} \qquad (49)$$

The constant Γ_o is determined at the point A where the slope of the curve of the shear-induced hydrostatic strain versus plastic shear strain is zero. (See Fig. 2). Then it follows from Eq. (49) that

$$\Gamma_o = \frac{\sigma_o}{s_A} \qquad (50)$$

where s_A is the value of s at point A in Fig. 2. Since the right-hand side of Eq. (49) is now known, $d\epsilon^p/de^p$ may be found for various values of k. The one which provides the best agreement with the experimental data is chosen.

Approximate Solution of Equation (49).

The hydrostatic response can be determined explicitly by means of an approximate solution of Eq. (43). In effect, since $\beta^* \exp(-\beta^* z_H)$ is close to a delta function, Eq. (43) becomes:

$$\sigma = e^{\beta\epsilon^p}\,\phi_o\left(1 - e^{-\beta^* z_H}\right) \qquad (51)$$

Thus

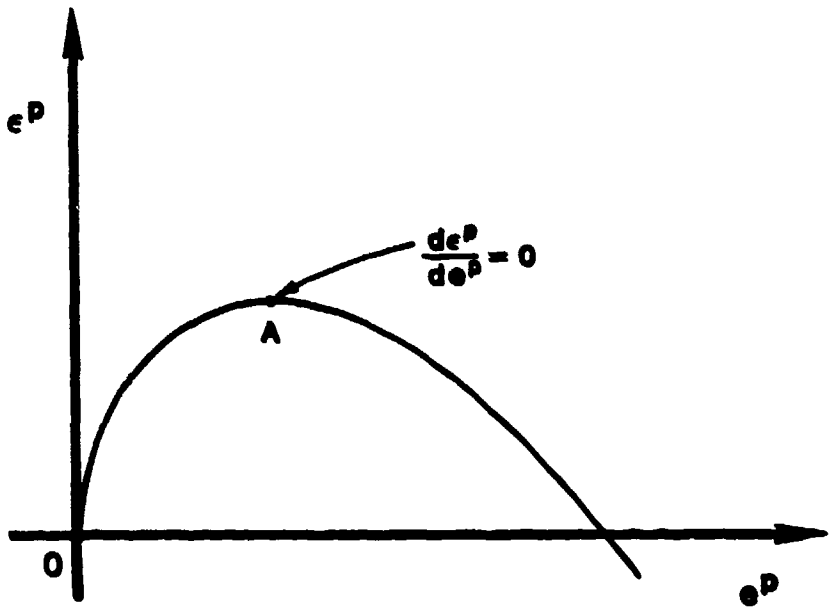

Figure 2. Shear-induced hydrostatic strain versus e^p.

$$\sigma_o = e^{\beta\epsilon_o^p}\,\phi_o\left(1 - e^{-\beta^* z_H^*}\right) \tag{52}$$

Equation (52) may now be used in Eq. (50) to give the following explicit result

$$k\,\frac{d\epsilon_D^p}{de^p} = \frac{1 - \Gamma_o^2\left(\frac{s}{\sigma_o}\right)^2}{D} \tag{53}$$

where

$$D = \frac{\Gamma_o\left(\frac{s}{\sigma_o}\right)}{1 - e^{-\beta^* z_H^*}} \cdot e^{\beta\epsilon_D^p} + \left[\left[\frac{e^{\beta\epsilon_D^p}}{1 - e^{-\beta^* z_H^*}}\right]^2 + \left(\frac{s}{\sigma_o}\,\Gamma_o\right)^2 - 1\right]^{1/2} \tag{54}$$

and

$$z_H^* = \frac{1}{\beta}\left(1 - e^{-\beta\epsilon_o^p}\right) \tag{55}$$

Solution of Eq. (49) for Asymptotically Small σ_o.

Of interest is the case of asymptotically small σ_o and ϵ_o^p in which event

$$z_H^* \sim \epsilon_o^p \tag{56}$$

and

$$1 - e^{-\beta^* z_H^*} \sim \beta^* z_H^* = \beta^* \epsilon_o^p \tag{57}$$

Thus Eq. (54) becomes

$$D = \frac{\Gamma_o\left(\frac{s}{\sigma_o}\right)}{\beta^* \epsilon_o^p} e^{\beta \epsilon_D^p} + \left[\frac{e^{2\beta \epsilon_D^p}}{\left(\beta^* \epsilon_D^p\right)^2} + \left(\frac{s}{\sigma_o} \Gamma_o\right)^2 - 1 \right]^{1/2} \tag{58}$$

It follows, therefore, that at small values of σ_o, D is magnified and thus the value of $d\epsilon_D^p/de^p$ is depressed and the onset of dilatancy is accelerated in accordance with observation.

2.3.5 The Shear Modulus G.

The singularity of the shear kernel ensures that the behavior is always elastic at loading, unloading and reloading points, on the shear stress-strain curve. Thus the initial shear modulus is determined by the slope of the tangent at the origin of the shear stress-strain curve. Measurement of this slope at other loading and unloading points will determine if G is constant. If not, then G will most likely depend on the second invariant of the elastic deviatoric shear strain tensor, i.e.,

$$G = G\left(\left|\left|\underset{\sim}{e}^e\right|\right|\right) \tag{59}$$

as was found to be the case in plain concrete (see Ref. 5). The form of the relationship will be found by measuring G at such points. In the present study G is considered constant and was determined from the initial slope of the shear stress-strain curve.

2.3.6 The Deviatoric Memory Kernel $\rho(z_D)$.

The kernel ρ is determined from the deviatoric response equation (12), i.e.,

$$s = \int_0^{z_D} \rho(z_D - z') \frac{de^p}{dz'} dz' \tag{60}$$

at a hydrostatic stress value σ_o at which the deviatoric hardening function F_D is normalized and equal to unity, i.e.,

$$F_D(\sigma_o) = 1 \tag{61}$$

The determination of F_D for other values of σ will be discussed shortly. Thus in the course of the shearing test conducted at $\sigma = \sigma_o$, we have

$$dz_D = dz \tag{62}$$

Now let z_o be the value of z at the conclusion of the hydrostatic test. Then in view of Eq. (62)

$$z_D = z - z_o \tag{63}$$

Also let the right-hand side of Eq. (49) be denoted by a function $\gamma(e^p)$. This function is known from experimental measurement. Thus

$$k \frac{d\epsilon^p}{de^p} = \gamma \tag{64}$$

Combining Eqs. (62) and (47) one finds the relation

$$\frac{de^p}{dz_D} = \frac{1}{(1 + \gamma^2)^{1/2}} \tag{65}$$

Integration of Eq. (65) yields the relation

$$e^p = e^p(z_D) \tag{66}$$

Let

$$\frac{de^p}{dz_D} \stackrel{def}{=} g(z_D) \tag{67}$$

where g is a known function of z_D. Also

$$s(e^p) = s\left[e^p(z_D)\right] = s(z_d) \tag{68}$$

In view of Eq. (60)

$$s(z_D) = \int_0^{z_D} \rho(z_D - z')g(z')dz' \tag{69}$$

Equation (69) is a Volterra integral equation of the first kind which can be solved for $\rho(z_D)$ since both s and g are known. The method of solution is given in Ref. 3.

2.3.7 Determination of the Hardening Function F_D.

The analysis behind the procedure was discussed at length in Ref. 5. Let s_∞ be the value of s in the limit of large e^p, in the course of a shear test at constant hydrostatic stress σ_o. Then it was shown in Ref. 5 that

$$F_D(\sigma_o) = \frac{s_\infty}{\sigma_o} \tag{70}$$

As a result, the dependence of F_D on σ_o, can be determined from data on shear tests conducted at several values of fixed hydrostatic pressure σ_o which span the hydrostatic range of interest.

Section 3

APPLICATION TO ISST SOIL DATA

In this section, the endochronic model described in Section 2.2 is applied to ISST soil, using the laboratory data for reconstitutied ISST soil generated by WES specifically for this study [4]. Before the model was fitted, the WES data were transformed from engineering strain to natural strain* so that the resulting model would be appropriate for use in conjunction with existing wave propagation codes, which typically are formulated in terms of natural strain. In addition, the volumetric strain was determined from the data in a consistent manner, using Eq. (1) given earlier. The material functions and parameters of the model were determined from the WES ISST data according to the methods described in Section 2.3. Specific details of the manner in which this was accomplished, as well as the results, are given below.

3.1 DETERMINATION OF HYDROSTATIC FUNCTIONS AND PARAMETERS.

The measured behavior of ISST soil to pure hydrostatic loading is shown in Figure 3, where the results from three separate tests have been plotted. As this figure reveals, the unloading-reloading paths practically coincide, indicating that the behavior along these paths is essentially elastic. In view of this, the dependence of the bulk modulus K on elastic volumetric strain ϵ^e (see Eq. (24)) was obtained from the unloading curve emanating from 57 MPa. The expression

$$K = K_0 + K_1 (\epsilon^e)^m \tag{71}$$

where

$$K_0 = 50 \text{ MPa}, \quad K_1 = 1.426 \times 10^{10} \text{ MPa}, \quad m = 5.2 \tag{72}$$

was found to describe the data very well.

---

* See Appendix A for details.

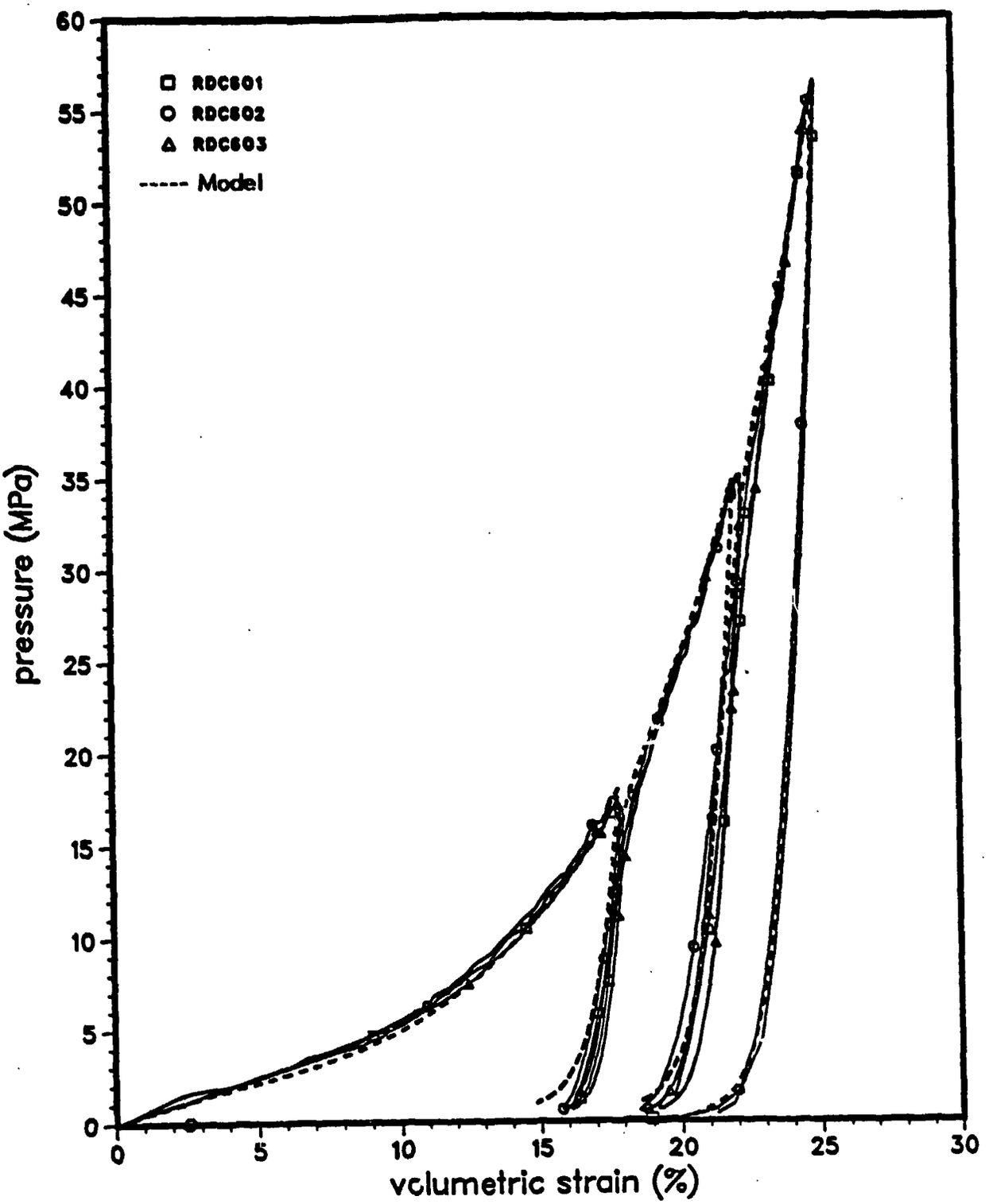

Figure 3. Isotropic compression of ISST soils, showing comparison between endochronic model and data.

The hydrostatic hardening function $F_H(\epsilon^p)$ was determined as follows. First, a plot of pressure, σ, versus plastic volumetric strain, ϵ^p, was constructed from the data shown in Figure 3, using the expression for the bulk modulus given in Eq. (71) to define the elastic volumetric strain. Since the unloading-reloading curves practically coincide, the kernel function $\phi(z_H)$ must be very close to a delta-function and, for the present purposes, was in fact assumed to be one. When this is the case, the virgin hydrostat is given by the expression (see Eq. (29)):

$$\sigma = \phi_o \, F_H(\epsilon^p) \tag{73}$$

This was fit to the σ versus ϵ^p data, using Eq. (30), with the result

$$F_H = e^{\beta\epsilon^p} \tag{74}$$

where

$$\beta = 19.5 \tag{75}$$

Turning now to the hydrostatic kernel function $\phi(z_H)$, we adopted the form given by Eq. (16), i.e.,

$$\phi(z_H) = \sum_{r=1}^{N} B_r e^{-\beta_r z_H} \tag{76}$$

and set N = 2. To determine the B_r and β_r, we proceeded as follows. First, let us set:

$$\eta(z_H) \equiv \sigma(z_H)(1 - \beta z_H) \tag{77}$$

A plot was made, in terms of $\eta(z_H)$ versus z_H, of the second reloading path shown in Figure 3. This plot shows that η approaches an asymptotic value, call it η_∞, as $z_H \to \infty$. A further plot was made of $\eta_\infty - \eta(z_H)$ versus z_H, and the resulting curve was fit, via Prony's method (see Ref. 14, for example), by an expression of the form:

$$\eta_\infty - \eta(z_H) = \sum_{r=1}^{2} C_r e^{-\beta_r z_H} \tag{78}$$

Differentiating this with respect to z_H, and recalling Eq. (38), it follows that

$$\phi(z_H) = \sum_{r=1}^{2} B_r e^{-\beta_r z_H} \tag{79}$$

where

$$B_r = \beta_r C_r \tag{80}$$

Thus since β_r and C_r are known from the Prony fit in Eq. (78), the B_r are also known as a result of Eq. (80). In this manner, the following values of B_r and β_r were determined:

$$\begin{aligned} B_1 &= 1{,}680 \text{ MPa} & \beta_1 &= 2{,}595. \\ B_2 &= 11{,}610 \text{ MPa} & \beta_2 &= 13{,}680. \end{aligned} \tag{81}$$

This completes the specification of the hydrostatic functions and parameters for ISST soil. A comparison between the model predictions based upon these functions and parameters and the corresponding WES soil data [4] is shown in Figure 3. As an inspection of this figure reveals, the model does a remarkably good job of capturing all of the details of the data.

3.2 DETERMINATION OF SHEAR-VOLUMETRIC COUPLING PARAMETERS k AND Γ_o.

For the determination of k and Γ_o, we will use Eq. (49) and the data given in Ref. 4 for the cases of shear at various fixed hydrostatic pressures. Attention is specifically focussed on the three cases for which the fixed hydrostatic pressure lies on the concave portion of the virgin hydrostat, i.e., those with fixed pressure of 3.45, 6.90 and 10.34 MPa.

The importance of Eq. (49) lies in the fact that by fitting it to the appropriate shear-volumetric coupling data obtained from shear tests at constant hydrostatic pressure, the values of the parameters k and Γ_o, can be found directly. Thus, the shear-volumetric coupling parameters do not need to be determined iteratively. It will be recalled that the parameter β was obtained independently from the pure hydrostatic compression data (see Eq. (75)) for ISST soils and has the value 19.5.

It should be noted that Eq. (49) was derived on the assumption that the shear strain increases monotonically. However, the shear tests at constant pressure reported in Ref. 4 were, for other reasons, not performed under monotonic shearing conditions. In each test, the shearing was interrupted at a shear strain of 3 percent by an unloading-reloading process, and then the shearing was continued out to a shear strain of about 11 percent, after which unloading took place. The experimental data for these tests are shown in Figures 4 to 6, where the volumetric strain due to shear has been plotted against the plastic octahedral shear strain. These figures reveal that the soil first undergoes compaction up to a peak, followed by dilatancy with further increases in the shear strain.

In applying Eq. (49) to the data depicted in Figures 4 to 6, we attempted to compensate for the effects of the unloading-reloading process at 3 percent shear strain. A numerical program was developed to integrate Eq. (49), and using this, the following values of k and Γ_o were found to provide the best correlation of the data from the three tests:

$$k = 0.6$$

$$\Gamma_o = 1.25 \text{ MPa}. \qquad (82)$$

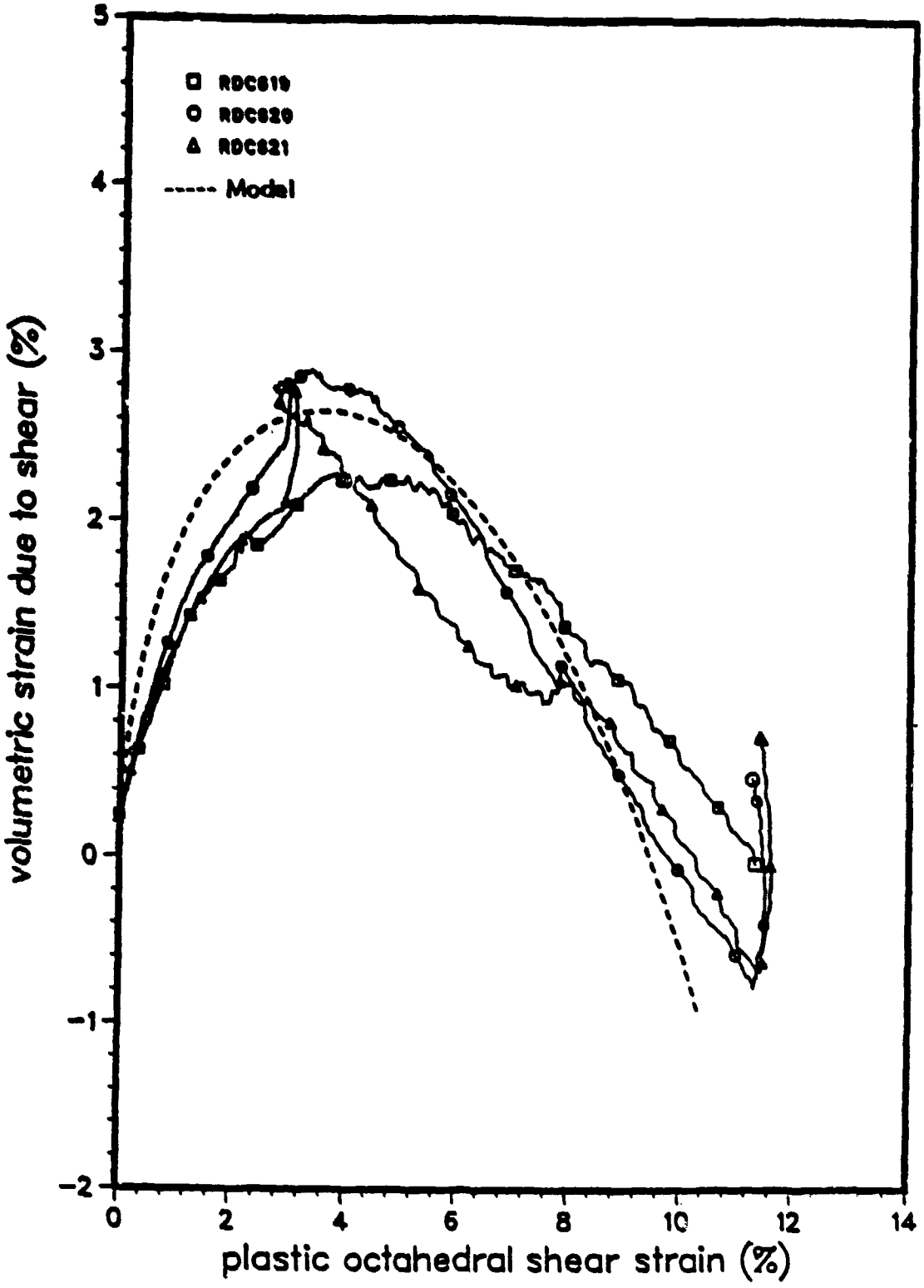

Figure 4. Shear-volumetric coupling at a fixed hydrostatic pressure of 3.45 MPa.

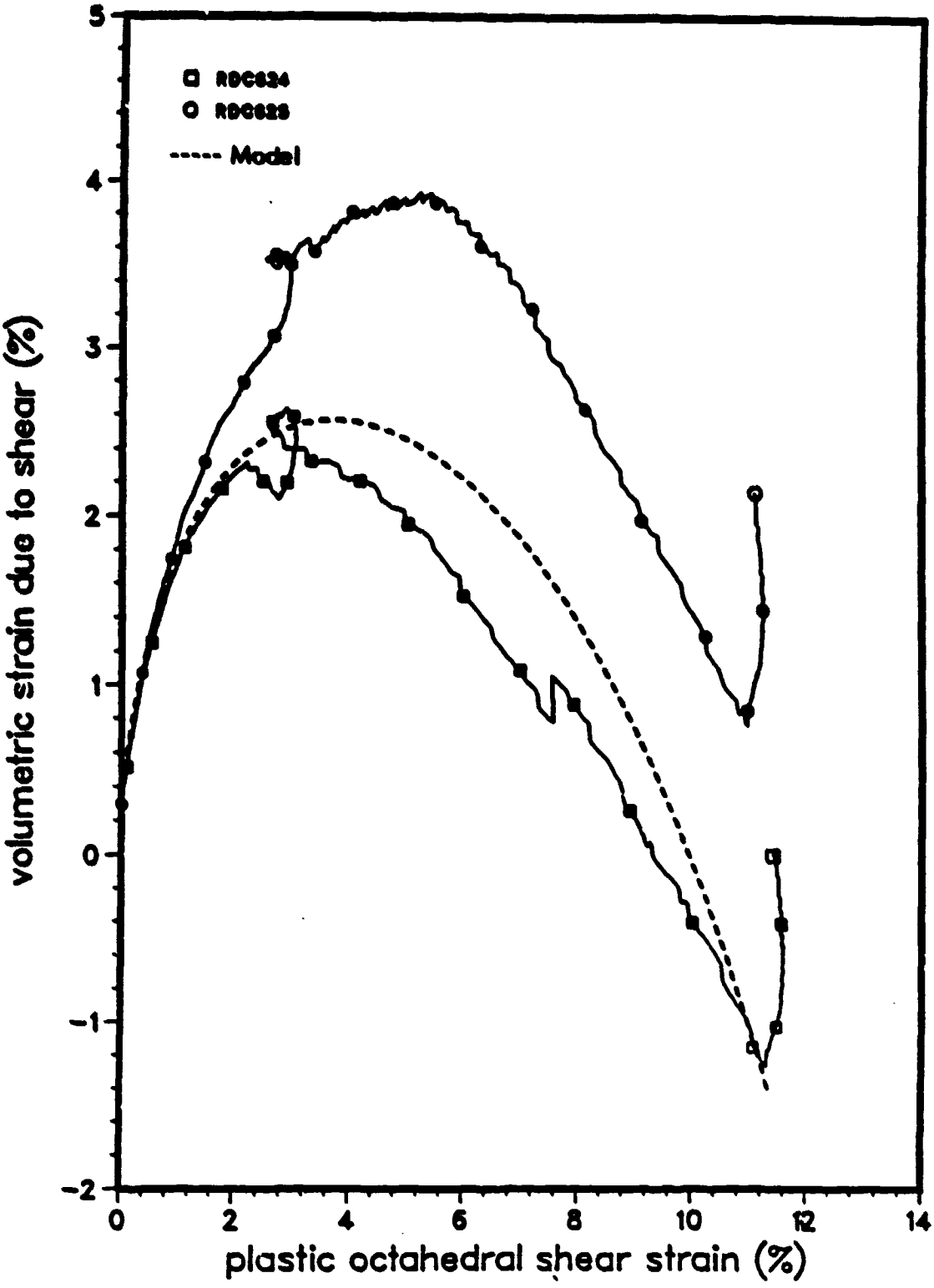

Figure 5. Shear-volumetric coupling at a fixed hydrostatic pressure of 6.90 MPa.

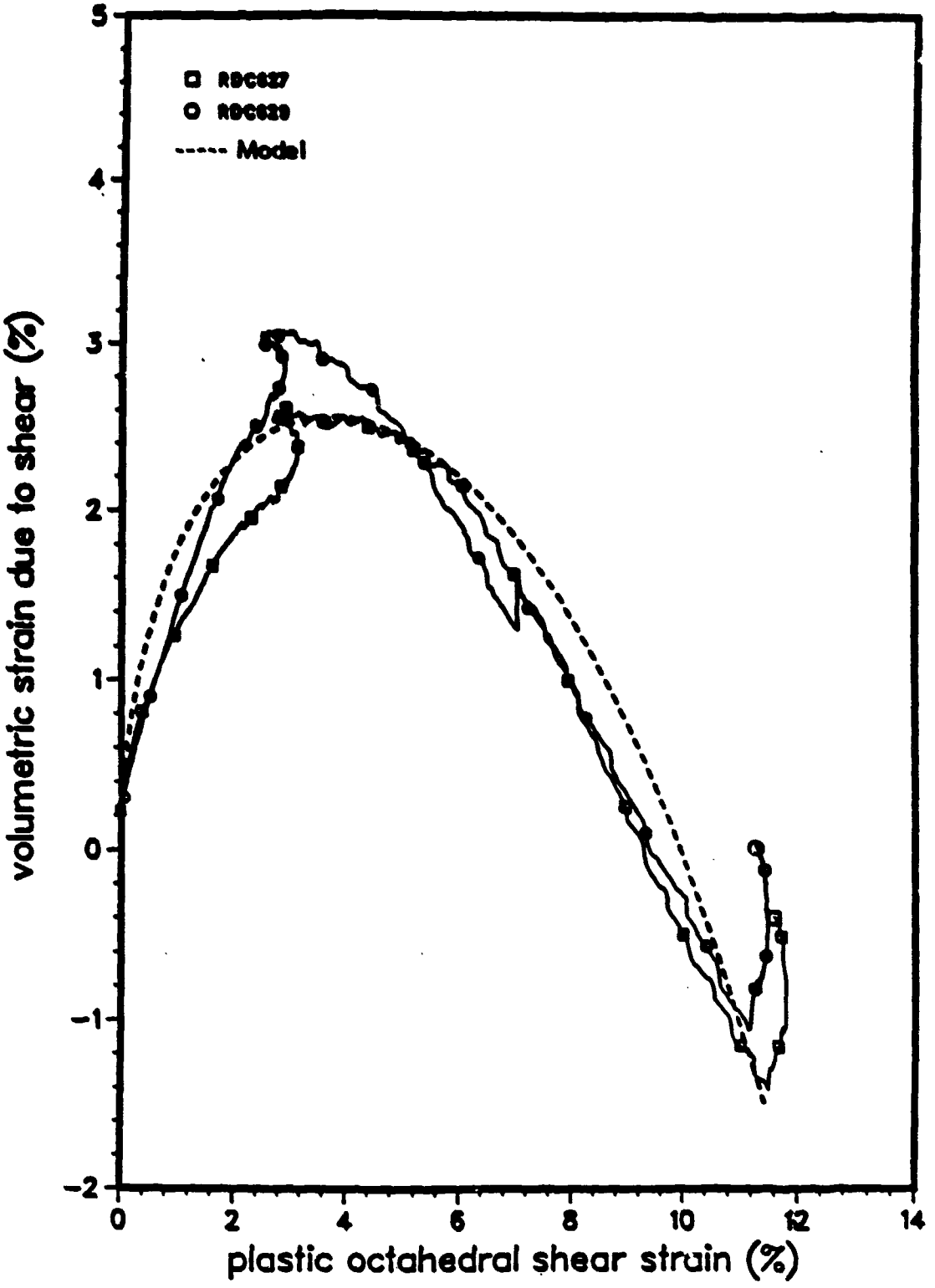

Figure 6. Shear-volumetric coupling at a fixed hydrostatic pressure of 10.34 MPa.

Figures 4 to 6 show comparisons between the data and Eq. (49) with the above values of the parameters. An inspection of these figures reveals that the model captures the essential features of the data quite well, in view of the fact that the data were not obtained under truly monotonic shearing conditions. These figures demonstrate the ability of the model to describe both compaction and dilatancy in accordance with experimental observation.

3.3 DETERMINATION OF DEVIATORIC FUNCTIONS AND PARAMETERS.

Figure 7 summarizes the measured dependencies of the octahedral shear stress on the octahedral shear strain from the nine shear tests reported in Ref. 4 that were performed at constant hydrostatic pressures. In view of the remarkable consistency and reproducibility of these data, the care with which these experiments were done is clearly evident.

The deviatoric functions G, $\rho(z_D)$ and F_D were determined from one of the tests depicted in Figure 7, namely, test RDC 624 in which the fixed hyhdrostatic pressure was 6.90 MPa. The volumetric strain caused by the shearing was taken to be irreversible (fully plastic) and, in the developments which follow, will be denoted by ϵ_D^p. From the data for test RDC 624, numerical tables of the relations

$$\tau = \tau(\gamma^p) \tag{83}$$

$$\epsilon_D^p = \epsilon_D^p(\gamma^p) \tag{84}$$

were constructed, where

$$\gamma^p = \gamma - \frac{\tau}{2G} \tag{85}$$

Here, τ and γ denote, respectively, the octahedral shear stress and the octahedral shear strain. Furthermore, γ^p is the plastic component of γ, while G is the shear modulus.

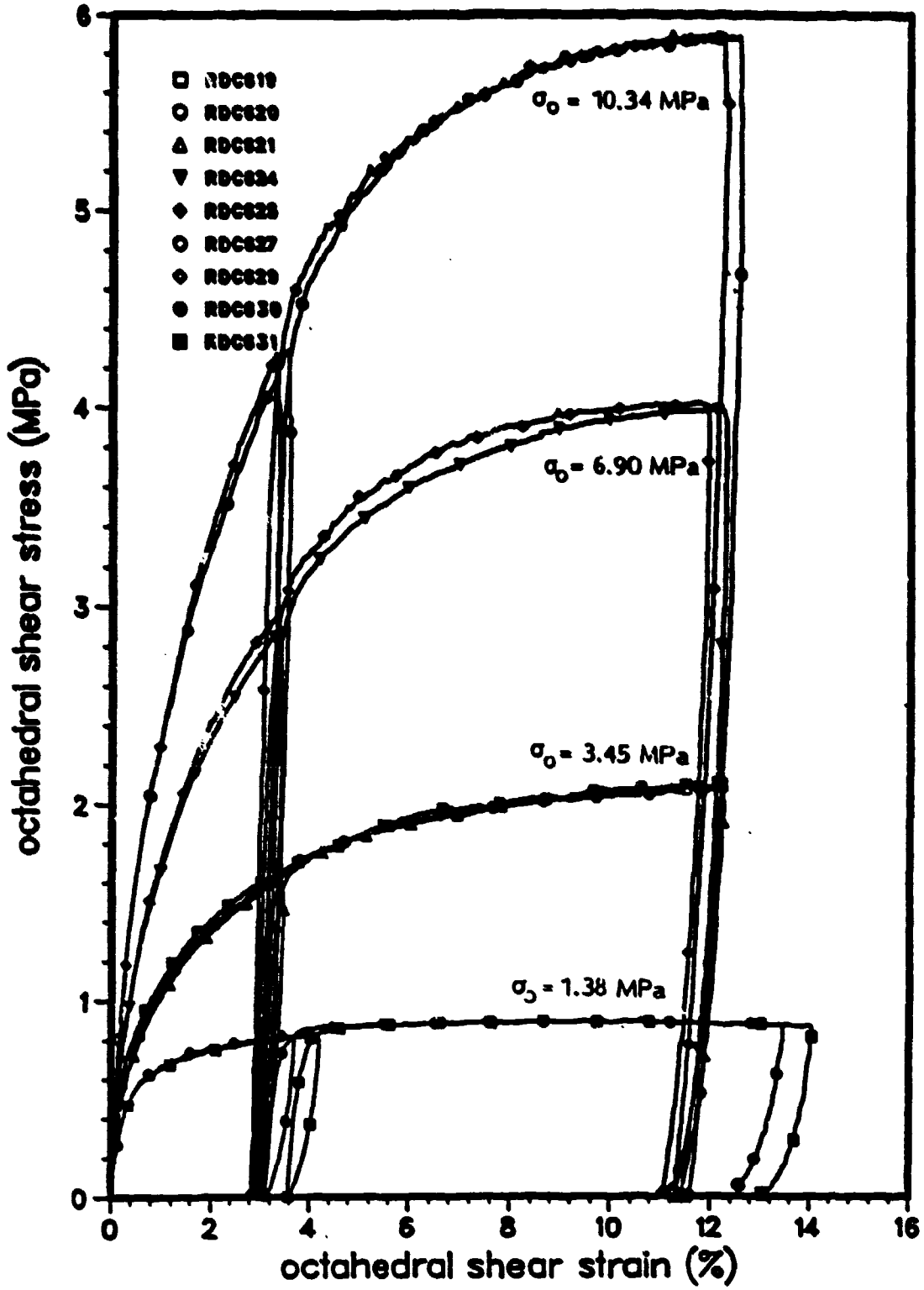

Figure 7. Octahedral shear stress versus octahedral shear strain for shear at several fixed hydrostatic pressures.

The shear modulus, and its dependence on γ, was found as follows. The response of the soil at the initiation of shear loading, as well as at the two points of unloading shown in Figure 7, is assumed to be purely elastic. On this basis, the slopes of the τ versus γ curve at these points defines the corresponding values of 2G. In this manner, the following dependence of 2G on γ was found to provide a reasonable description of the data:

$$2G = 2G_o + c_o\sqrt{\gamma} \tag{86}$$

where

$$\begin{aligned} 2G_o &= 500 \text{ MPa} \\ c_o &= 3000 \text{ MPa} \end{aligned} \tag{87}$$

To determine the kernel function $\rho(z_D)$, we begin by rewriting Eq. (69) in the form

$$\tau(w) = \int_o^w \rho(w - w')\frac{d\gamma^p}{dw'}\,dw' \tag{88}$$

where τ and γ^p are, respectively, the octahedral shear stress and plastic octahedral shear strain,

$$w \equiv z_D - z_D^o \quad , \tag{89}$$

and z_D^o denotes the value of z_D at the end of the pure hydrostatic compression phase of the test. In Eq. (88), $\tau(w)$ and $d\gamma^p/dw(w)$ are presumed known while $\rho(w)$ is to be determined. To determine $\tau(w)$ and $d\gamma^p/dw(w)$, the relation between γ^p and w during shearing must be known. This relation was found by numerically integrating Eq. (49), which can be rewritten in the form:

$$dw = \frac{\left[e^{2\beta\epsilon_D^p} + 3\left[\frac{\Gamma_o}{\sigma_o}\tau\right]^2\right] d\gamma^p}{\left\{\frac{\Gamma_o}{\sigma_o}\tau + \frac{1}{\sqrt{3}}e^{\beta\epsilon_D^p}\left[e^{2\beta\epsilon_D^p} + 3\left[\frac{\Gamma_o}{\sigma_o}\tau\right]^2 - 1\right]^{1/2}\right\}} \tag{90}$$

Inasmuch as both τ and ϵ_D^p are known as functions of γ^p from Eqs. (83) and (84), the righthand side of Eq. (90) can be expressed solely in terms of γ^p, i.e., Eq. (90) can be written in the form:

$$dw = \phi(\gamma^p)d\gamma^p \tag{91}$$

and numerically integrated to give the relation

$$w = w(\gamma^p) \tag{92}$$

In this manner, the relation between w and γ^p, shown in Figure 8, was obtained. The relation (92) was numerically inverted to give

$$\gamma^p = \gamma^p(w) \tag{93}$$

Therefore, by using Eq. (93), the relations (83) and (84) were expressed in the form:

$$\tau = \tau(w)$$

$$\frac{d\gamma^p}{dw} = \frac{d\gamma^p}{dw}(w) \tag{94}$$

Using these relations in conjunction with Eq. (88), the resulting Volterra integral equation was solved numerically for $\rho(w)$, using a technique described in Ref. 3. The result was then fit by Prony's method [14] to yield the following expression for the shear kernel function:

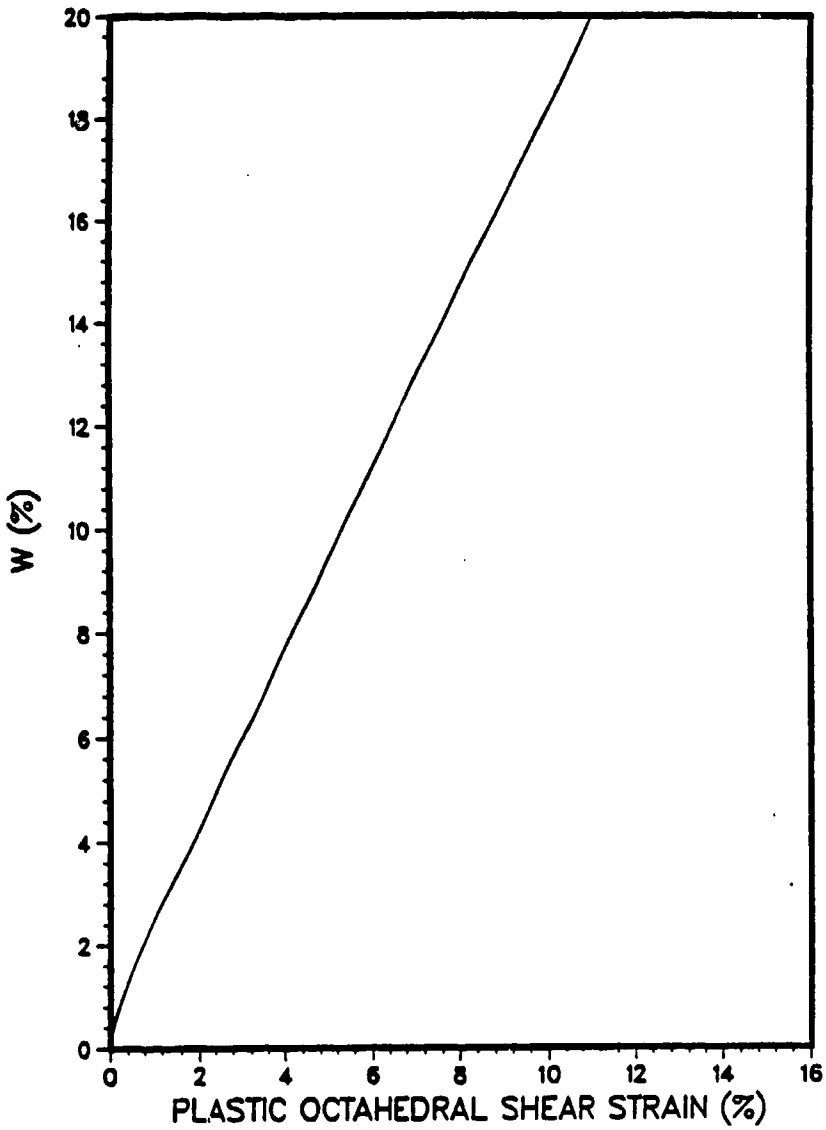

Figure 8. W as a function of γ^p for test RDC 624.

$$\rho(z_D) = \sum_{r=1}^{3} A_r e^{-\alpha_r z_D} \tag{95}$$

where

$$A_1 = 11.6 \text{ MPa} \qquad \alpha_1 = 9.0$$
$$A_2 = 160 \text{ MPa} \qquad \alpha_2 = 28.9 \tag{96}$$
$$A_3 = 706 \text{ MPa} \qquad \alpha_3 = 1,381.$$

To provide a check on the internal consistency of the above operations, we performed the following analysis. The expression given by Eq. (95) for $\rho(z_D)$, together with the derivative $d\gamma^p/dw$ obtained from the relation between γ^p and w depicted in Figure 8, were used in conjunction with Eq. (88) to predict $\tau(w)$. Figure 9 shows a comparison between the predicted $\tau(w)$ and the coresponding $\tau(w)$ from the data for test RDC 624. As the figure reveals, the agreement is quite good and thus validates the accuracy of the above technique.

To determine the shear hardening function, F_D, we first recall that in the preceding devlopments we set $F_D = 1$ at the reference pressure of $\sigma_R = 6.90$ MPa. In view of this, we can write Eq. (70) as

$$F_D(\sigma_o) = \frac{\tau_{ss}(\sigma_o)}{\tau_{ss}(\sigma_R)} , \tag{97}$$

since s_{ss} and τ_{ss} differ only by a multiplicative constant. The dependence of τ_{ss} on σ_o, for the ISST soil, is given by the data in Figure 10 and is found to have the following linear form:

$$\tau_{ss}(\sigma_o) = \tau_s + \beta_s \sigma_o \tag{98}$$

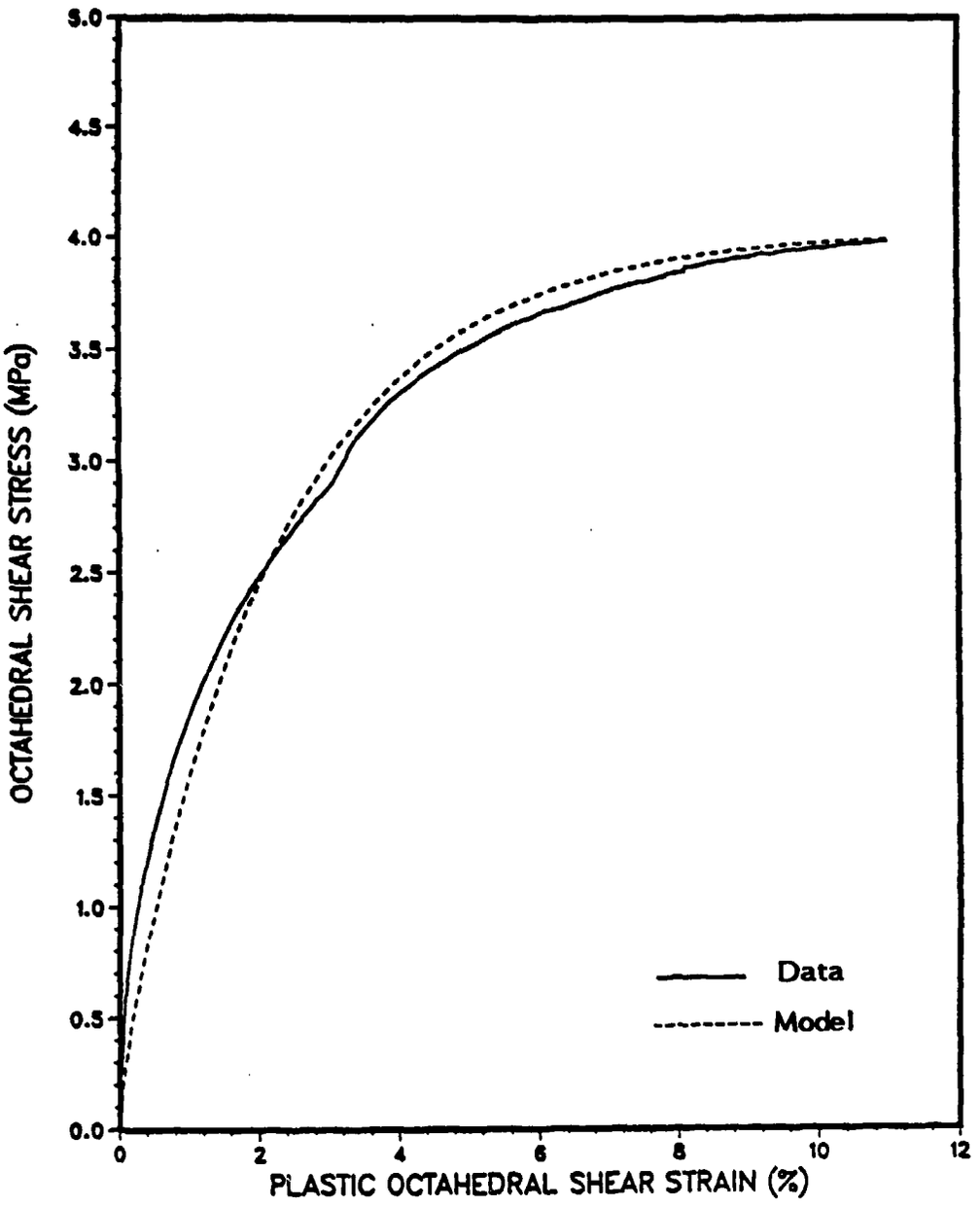

Figure 9. τ versus γ^p for test RDC 624, showing comparison between model prediction and data.

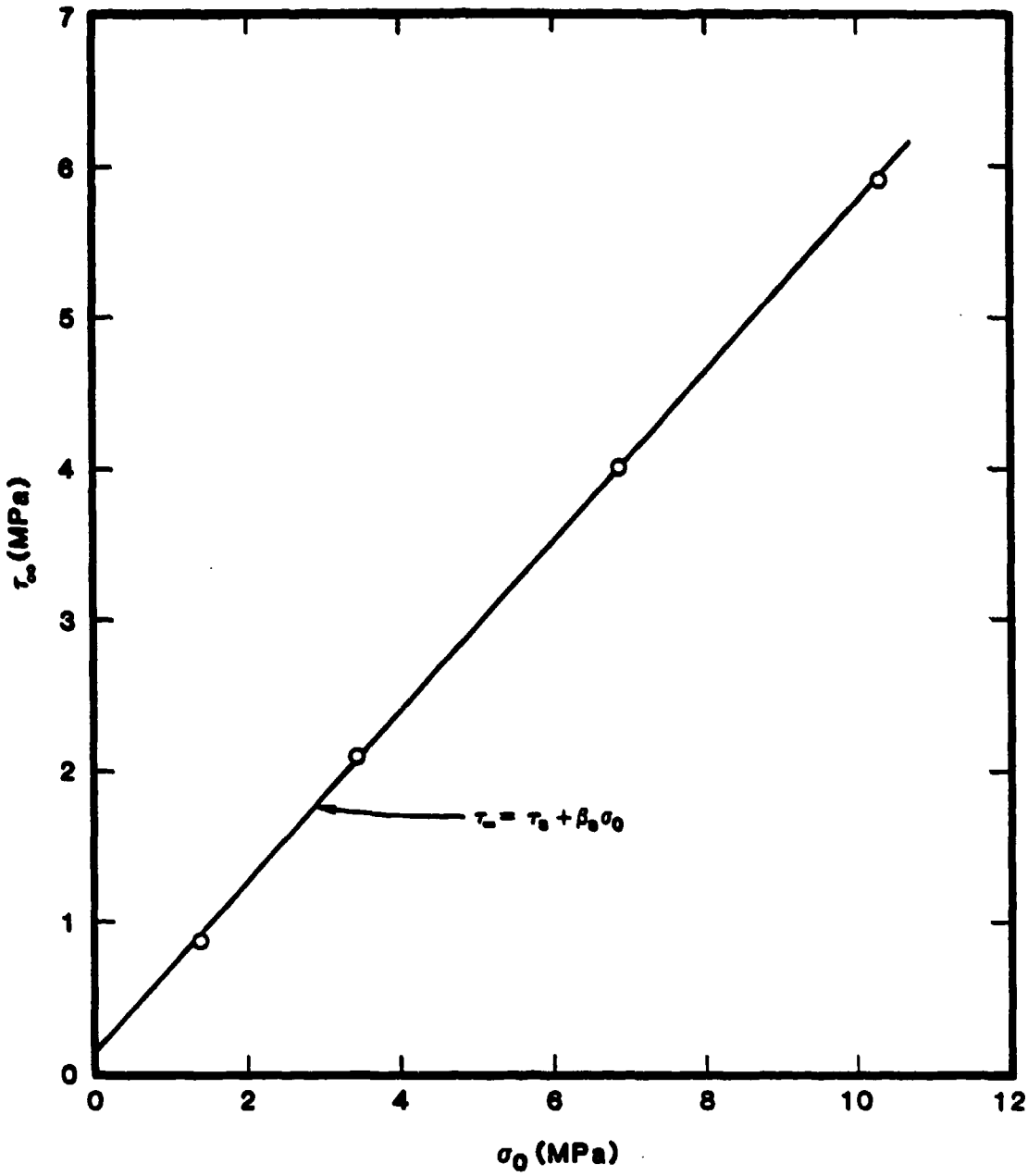

Figure 10. τ_∞ versus σ_0 for ISST soils. The circles denote data points from Ref. 4.

where

$$\tau_s = 0.15 \text{ MPa}$$

$$\beta_s = 0.56 \tag{99}$$

For the reference pressure of 6.9 MPa, we find from Figure 7 that

$$\tau_\infty(\sigma_o) = 4.0 \text{ MPa} \tag{100}$$

Thus, from Eqs. (97) to (100), it follows that

$$F_D = \phi_o + \phi_1 \sigma \tag{101}$$

where

$$\phi_o = 0.0375$$

$$\phi_1 = 0.140 \text{ MPa}^{-1} \tag{102}$$

The specification of the model parameters for the ISST soil is now complete.

Section 4

NUMERICAL CONSIDERATIONS

A numerical scheme is presented in this section for integrating the system of equations which govern the new endochronic model with dilatancy described in Section 2.2. The scheme is explicit, first order accurate* and based upon Euler's method. Accordingly, care must be taken in applying the method to ensure that the prescribed increments are sufficiently small so that the computed results are essentially independent of the increment size. Otherwise, the scheme is straightforward, efficient and easy to implement.

Two different versions of the scheme are described below, namely, one which requires the prescribed strain history as input and one which requires the prescribed stress history as input. In both cases, the equations are restricted to principal directions of stress and strain. Another version that specifically applies to the standard triaxial compression configuration has been developed under separate contract [16]. A listing of a computer program for the version of the scheme that requires the prescribed strain history as input is given in Appendix B.

4.1 BASIC EQUATIONS.

The basic equations which govern the new endochronic soil model with dilatancy were given earlier in Section 2.2 but are summarized below for convenience;

$$\underline{\xi} = \int_0^{z_D} \rho(z_D - z') \frac{d\underline{e}^p}{dz'} \, dz' \tag{103}$$

$$\sigma = \int_0^{z_H} \phi(z_H - z') \frac{d\epsilon^p}{dz'} \, dz' + \int_0^{z_H} \Gamma(z_H - z') \, \underline{\xi} \cdot \frac{d\underline{e}^p}{dz'} \, dz' \tag{104}$$

---

* A second-order accurate scheme has recently been developed by Murakami and Read [15].

$$d\underline{s} = 2G\left(d\underline{e} - d\underline{e}^{p}\right) \tag{105}$$

$$d\sigma = K\left(d\epsilon - d\epsilon^{p}\right) \tag{106}$$

$$dz^2 = \left|\left|d\underline{e}^{p}\right|\right|^2 + k^2\left(d\epsilon^{p}\right)^2 \tag{107}$$

$$dz_D = dz/F_D \tag{108}$$

$$dz_H = dz/\left(kF_H\right) \tag{109}$$

Here, $\underline{s}$ denotes the deviatoric stress tensor, σ is the hydrostatic stress (pressure), $\underline{e}^{p}$ represents the plastic component of the deviatoric strain tensor $\underline{e}$, while ϵ^{p} is the plastic component of the volumetric strain ϵ. Moreover, G and K are, respectively, the shear and bulk moduli, while k is a contant which determines the magnitude of shear-volumetric coupling. The double bars surrounding a symbol denote its Euclidean norm, while single bars denote absolute value. Furthermore, F_D and F_H are, respectively, shear and hydrostatic hardening functions. In addition, z denotes the intrinsic time scale, while z_D and z_H are, respectively, the intrinsic times for shear, dilatancy and hydrostatic behavior. Finally, $\rho(z)$, $\phi(z)$ and $\Gamma(z)$ are weakly singular kernel functions satisfying the condition $\rho(0) = \phi(0) = \Gamma(0) = \infty$, but integrable in the domain $0 \leq z < \infty$.

The weakly singular kernel functions can be expressed in terms of Dirichlet series:

$$\rho(z) = \sum_{r=1}^{\infty} A_r e^{-\alpha_r z} \tag{110}$$

$$\phi(z) = \sum_{i=1}^{\infty} B_i e^{-\beta_i z} \tag{111}$$

$$\Gamma(z) = \sum_{i=1}^{\infty} \Gamma_i e^{-\eta_i z} \tag{112}$$

where in order to satisfy the Clausius-Duhem inequality, it is necessary that $\alpha_r \geq 0$, $\beta_i \geq 0$, $\eta_i \geq 0$ and $A_r \geq 0$, $B_i \geq 0$, $\Gamma_i \geq 0$. Moreover, to ensure that $\rho(z)$, $\phi(z)$ and $\Gamma(z)$ are singular at the origin and integrable over a finite domain, we must have

$$\sum_{r=1}^{\infty} A_r = \sum_{i=1}^{\infty} B_i = \sum_{i=1}^{\infty} \Gamma_i = \infty \tag{113}$$

and

$$\sum_{r=1}^{\infty} A_r/\alpha_r < \infty \ , \ \sum_{i=1}^{\infty} B_i \ / \ \beta_i < \infty \ \ , \ \sum_{i=1}^{\infty} \Gamma_i/\eta_i = \infty \tag{114}$$

4.2 INCREMENTAL FORM OF BASIC EQUATIONS.

In applications of the theory to date, it has been found that two or three terms of the series (110) to (112) are usually quite adequate for representing the kernel functions. In such cases, however, care must be taken to ensure that the infinitely large values of $\rho(0)$, $\phi(0)$ and $\Gamma(0)$ are approximated by suitably large finite values. When this is done, we can write:

$$\rho(z) \doteq \sum_{r=1}^{n} A_r \ e^{-\alpha_r z} \tag{115}$$

$$\phi(z) \doteq \sum_{i=1}^{m} B_i e^{-\beta_i z}$$

$$\Gamma(z) \doteq \sum_{i=1}^{m} \Gamma_i \, e^{-\gamma_i z} \tag{116}$$

where n and m are finite.

It then follows that the expressions for $\underline{\underline{s}}$ and σ, as given by Eqs. (103) and (104), can be alternately written as

$$\underline{\underline{s}} = \sum_{r=1}^{n} \underline{\underline{Q}}_r \tag{117}$$

$$\sigma = \sum_{i=1}^{m} P_i + \sum_{i=1}^{m} N_i \tag{118}$$

where $\underline{\underline{Q}}_i$, P_i and N_i satisfy the following ordinary differential equations:

$$\frac{d\underline{\underline{Q}}_r}{dz_D} + \alpha_r \underline{\underline{Q}}_r = A_r \frac{d\underline{\underline{e}}^p}{dz_D} \qquad r = 1,2,\ldots,n \tag{119}$$

$$\frac{dP_i}{dz_H} + \beta_i P_i = B_i \frac{d\epsilon^p}{dz_H} \qquad i = 1,2,\ldots,m \tag{120}$$

$$\frac{dN_i}{dz_H} + \gamma_i N_i = \Gamma_i \left(\underline{\underline{s}} \cdot \frac{d\underline{\underline{e}}^p}{dz_H} \right) \qquad i = 1,2,\ldots,m \tag{121}$$

From Eqs. (117) to (121) we can write:

$$d\underset{\sim}{\xi} = A\, d\underset{\sim}{\varepsilon}^{p} \cdot \underset{\sim}{Q}\, dz_{D} \tag{122}$$

$$d\sigma = B\, d\epsilon^{p} + \Gamma\left(\underset{\sim}{\xi} \bullet d\underset{\sim}{\varepsilon}^{p}\right) \cdot (P + N)\, dz_{H} \tag{123}$$

where

$$A = \sum_{r=1}^{n} A_r \qquad \Gamma = \sum_{i=1}^{m} \Gamma_i$$

$$\underset{\sim}{Q} = \sum_{r=1}^{n} e_r\, \underset{\sim}{Q}_r \qquad N = \sum_{i=1}^{m} \gamma_i\, N_i \tag{124}$$

$$B = \sum_{i=1}^{m} B_i \qquad P = \sum_{i=1}^{m} \beta_i\, P_i$$

Equations (122) and (123) provide a simple approach for incrementally integrating the stresses $\underset{\sim}{\xi}$ and σ, which is considerably more attractive from a computational standpoint than numerically coping with the hereditary integrals in Eqs. (103) and (104).

In that which follows, explicit numerical schemes are presented for incrementally updating the endochronic equations given above when either the strain incrments or the stress increments are given. Because of the explicit nature of the scheme, it is necessary that the increments be taken sufficiently small to ensure accuracy.

4.3 PRESCRIBED STRAIN INCREMENTS $\Delta\underset{\sim}{\varepsilon}$.

It is assumed that $\underset{\sim}{\xi}$, σ, $\underset{\sim}{\varepsilon}$, $\underset{\sim}{\varepsilon}^{p}$, ϵ, ϵ^{p}, $\underset{\sim}{Q}_r$, N_i and P_i are known at the beginning of each prescribed strain incrment, $\Delta\underset{\sim}{\varepsilon}$. From Eqs. (108), (109), (122) and (123), we can write

$$\Delta \underset{\sim}{\varepsilon} = A\, \Delta \underset{\sim}{e}^{p} - \underset{\sim}{Q}\, \frac{\Delta z}{F_D} \tag{125}$$

$$\Delta \sigma = B\, \Delta \epsilon^{p} + \Gamma \left(\underset{\sim}{s} \cdot \Delta \underset{\sim}{e}^{p} \right) - \left(\frac{P + N}{k F_H} \right) \Delta z \tag{126}$$

If we now combine these equations with the incremental Hooke's Law, Eqs. (105) and (106), it follows that

$$\Delta \underset{\sim}{e}^{p} = \frac{1}{(A + 2G)} \left[2G\, \Delta \underset{\sim}{e} + \underset{\sim}{Q}\, \frac{\Delta z}{F_D} \right] \tag{127}$$

$$\Delta \epsilon^{p} = \frac{1}{(B + K)} \left\{ K \Delta \epsilon - \frac{2G\, \Gamma}{A + 2G} \left(\underset{\sim}{s} \cdot \Delta \underset{\sim}{e} \right) + \left[\frac{P + N}{k F_H} - \frac{\Gamma \left(\underset{\sim}{Q} \cdot \underset{\sim}{s} \right)}{(A + 2G) F_D} \right] \Delta z \right\} \tag{128}$$

Upon substituting these results into Eq. (107), the following quadratic expression for Δz is obtained:

$$a\, \Delta z^2 + b\, \Delta z + c = 0 \quad . \tag{129}$$

where

$$a = 1 - \frac{\underset{\sim}{Q} \cdot \underset{\sim}{Q}}{(A + 2G)^2 F_D^2} - \frac{1}{(B + K)^2} \left[\frac{P + N}{F_H} - \frac{k \Gamma \left(\underset{\sim}{Q} \cdot \underset{\sim}{s} \right)}{(A + 2G) F_D} \right]^2 \tag{130}$$

$$b = -2 \left\{ \frac{2G\, \underset{\sim}{Q} \cdot \Delta \underset{\sim}{e}}{(A + 2G)^2 F_D} - \frac{k^2}{(B + K)^2} \left[\frac{P + N}{k F_H} - \frac{\Gamma \left(\underset{\sim}{Q} \cdot \underset{\sim}{s} \right)}{(A + 2G) F_D} \right] \left[\frac{2G\, \Gamma}{A + 2G} \left(\underset{\sim}{s} \cdot \Delta \underset{\sim}{e} \right) - K \Delta \epsilon \right] \right\} \tag{131}$$

$$c = -\left\{\left[\frac{2G}{A+2G}\right]^2 \Delta\underline{\xi} \cdot \Delta\underline{\xi} + \frac{K^2}{(B+K)^2}\left[K\Delta\epsilon - \frac{2G\,\Gamma}{A+2G}\left(\underline{\xi}\cdot\Delta\underline{\xi}\right)\right]^2\right\} \tag{132}$$

It can be verified that the above expression for a, b, and c reduce to those given in Ref. 17 when dilatancy is not present, i.e., $N = \Gamma = 0$. Equation (129) provides two roots $\Delta z_{1,2}$, the one of interest being the one for which $\Delta z \geq 0$. Once Δz is known, $\Delta\underline{\xi}^p$ and $\Delta\epsilon^p$ can be obtained from Eqs. (127) and (128), after which $\Delta\underline{\xi}$ and $\Delta\sigma$ can be obtained from Eqs. (125) and (126). Finally, Eqs. (119) to (121) are used to update the $\underline{Q}_\Gamma$, N_i and P_i. This approach, therefore, permits one to determine the stress increments, $\Delta\underline{\xi}$, for prescribed increments in the strain $\Delta\underline{\xi}$.

4.4 PRESCRIBED STRESS INCREMENTS $\Delta\underline{\xi}$.

In this case, $\underline{\xi}$, σ, $\underline{\xi}$, $\underline{\xi}^p$, ϵ, ϵ^p, $\underline{Q}_\Gamma$, N_i and P_i are assumed to be known at the beginning of each prescribed stress increment $\Delta\underline{\xi}$. From Eqs. (109), (122) and (123), we can obtain the expressions:

$$\Delta\underline{\xi}^p = \frac{1}{A}\left[\Delta\underline{\xi} + \frac{\underline{Q}}{F_D}\Delta z\right] \tag{133}$$

$$\Delta\epsilon^p = \frac{1}{B}\left[\Delta\sigma - \frac{\Gamma}{A}\left(\underline{\xi}\cdot\Delta\underline{\xi}\right) + \left[\frac{P+N}{kF_H} - \frac{\Gamma}{A}\frac{\left(\underline{Q}\cdot\underline{\xi}\right)}{F_D}\right]\Delta z\right] \tag{134}$$

Upon substituting these results into Eq. (107), we obtain the following quadratic expression for Δz:

$$a\,\Delta z^2 + b\,\Delta z + c = 0 \tag{135}$$

where

$$a = 1 - \frac{\underset{\sim}{Q} \cdot \underset{\sim}{Q}}{(A F_D)^2} - \frac{1}{B^2}\left[\frac{P + N}{F_H} - \frac{k\Gamma(\underset{\sim}{Q} \cdot \underset{\sim}{S})}{A F_D}\right]^2 \tag{136}$$

$$b = -2\left\{\frac{\underset{\sim}{Q} \cdot \Delta\underset{\sim}{S}}{A^2 F_D} + \left(\frac{k}{B}\right)^2\left[\Delta\sigma - \frac{\Gamma}{A}(\underset{\sim}{S} \cdot \Delta\underset{\sim}{S})\right]\left[\frac{P + N}{k F_H} - \frac{\Gamma(\underset{\sim}{Q} \cdot \underset{\sim}{S})}{A F_D}\right]\right\} \tag{137}$$

$$c = -\left\{\frac{\Delta\underset{\sim}{S} \cdot \Delta\underset{\sim}{S}}{A^2} + \left(\frac{k}{B}\right)^2\left[\Delta\sigma - \frac{\Gamma}{A}(\underset{\sim}{S} \cdot \Delta\underset{\sim}{S})\right]^2\right\} \tag{138}$$

Again, the root of interest from Eq. (135) is that for which $\Delta z \geq 0$. Once Δz is found from Eq. (135), $\Delta\underset{\sim}{e}$ and $\Delta\epsilon^p$ can be determined from (133) and (134), after which $\Delta\underset{\sim}{e}$ and $\Delta\epsilon$ may be found from Eqs. (105) and (106). The $\underset{\sim}{Q}_\Gamma$, N_i and the P_i are updated on the basis of Eqs. (119) to (121). This approach, therefore, permits one to determine the strain increments $\Delta\underset{\sim}{\varepsilon}$ for prescribed increments in the stress $\Delta\underset{\sim}{\sigma}$.

Section 5

NUMERICAL ANALYSIS OF SHEAR AT FIXED HYDROSTATIC PRESSURE

In order to provide a check on the accuracy of (1) the numerical scheme, (2) the computer program, and (3) the material functions and parameters that had been determined for ISST soil, we conducted a computer study of the four test cases of shear at fixed hydrostatic pressure reported by WES in Reference 4. The stress-drive version of the numerical scheme, described in Section 4.4, was used for this purpose, since the corresponding laboratory tests had been conducted under stress-controlled conditions. The general stress path followed by these tests in the Rendulic plane is depicted in Figure 11, which shows the four legs consisting of (1) pure hydrostatic loading up to some fixed hydrostatic pressure σ_o, (2) shear loading at fixed σ_o, (3) shear unloading at fixed σ_o, and (4) pure hydrostatic unloading.

5.1 DESCRIPTION OF DIFFICULTY.

The numerical calculations proceeded smoothly and gave satisfactory results for the first three legs. However, on the fourth leg, which involved pure hydrostatic unloading, difficulties typically arose after the hydrostatic pressure had been reduced from between 20 to 25 percent of its peak value σ_o. To elaborate on the difficulty in greater detail, let us first recall that, in the case of the stress-driven numerical algorithm, the increment in the intrinsic time Δz is determined from the quadratic expression given by Eq. (135), i.e.,

$$a\,\Delta z^2 + b\,\Delta z + c = 0 \tag{139}$$

where a, b and c are defined by Eqs. (136) to (138), but may be alternately expressed in the following form:

$$a = 1 - \frac{\overset{*}{Q} \cdot \overset{*}{Q}}{(A\,F_D)^2} \cdot \left[\frac{P^*}{B\,F_H}\right]^2 \tag{140}$$

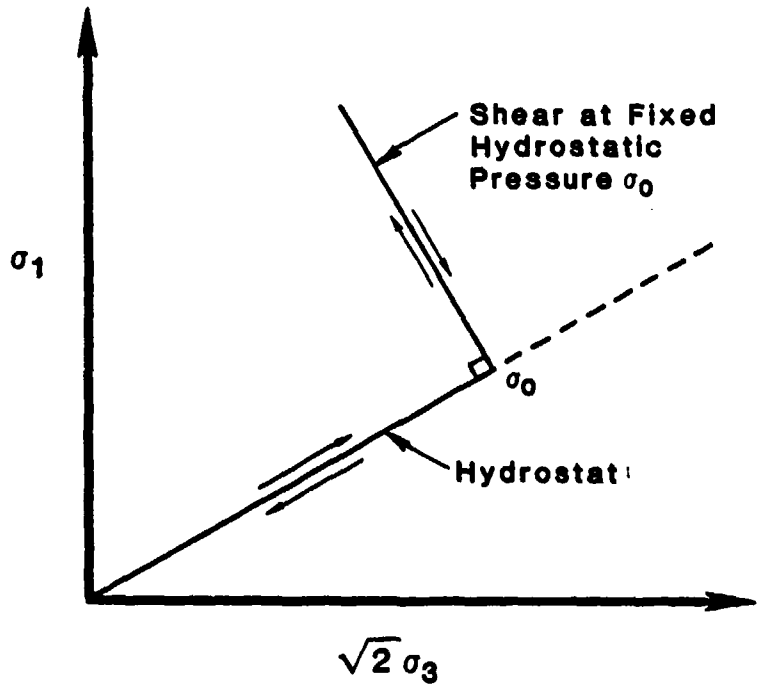

Figure 11 Description of stress path in Rendulic plane for WES tests of shear at fixed hydrostatic pressure.

$$b = -2\left\{\frac{\underset{\sim}{Q}\cdot\Delta\underset{\sim}{s}}{A^2} + \frac{k\,P^*}{B^2\,F_H}\,\Delta\sigma^*\right\} \tag{141}$$

$$c = -\left\{\frac{\Delta\underset{\sim}{s}\cdot\Delta\underset{\sim}{s}}{A^2} + \left(\frac{k\,\Delta\sigma}{B}\right)^2\right\}, \tag{142}$$

if we set

$$\Delta\sigma^* = \Delta\sigma - \frac{\Gamma}{F_H}\left(\underset{\sim}{s}\cdot\Delta\underset{\sim}{s}\right) \tag{143}$$

$$P^* = P - \frac{\Gamma}{F_D}\left(\underset{\sim}{s}\cdot\underset{\sim}{Q}\right) \tag{144}$$

Inasmuch as Δz is, by definition, unique and positive, an admissible solution of Eq. (139) is obtained when the two roots, Δz, and Δz_2, are real, unequal and of opposite sign. When this is the case, Δz is defined by the positive root, and the negative root is considered redundant. An admissible solution is therefore obtained when the following inequalities are satisfied:

$$b^2 - 4ac > 0 \tag{145}$$

$$c/a < 0 \tag{146}$$

Note from Eq. (142) that the parameter c is always negative. The parameter b may be either positive or negative. Thus, if $a < 0$ then either real roots Δz do not exist, or they both have the same sign. Either of these two cases is inadmissible and the computer program was designed to stop if this situation arose. The parameter a must be positive if an admissible solution is to be obtained.

For the cases of shear at constant hydrostatic pressure that we studied numerically, the parameter a became negative in the early stages of the hydrostatic unloading leg and, when this occurred, the computer program stopped. To obtain an understanding of how this can occur, let us examine the governing equation for Δz on this leg. Note that for hydrostatic unloading under zero shear, $\Delta \underset{\sim}{s} = 0$ so that $\Delta\sigma^* = \Delta\sigma$. In this case, the solution of the quadratic equation (139) yields the following result:

$$\Delta z = \frac{k\,\Delta\sigma}{B}\left\{\frac{\frac{P^*}{B\,F_H} + \sqrt{1 - \left\|\frac{\underset{\sim}{Q}}{A\,F_D}\right\|^2}}{1 - \left(\frac{P^*}{B\,F_H}\right)^2 - \left\|\frac{\underset{\sim}{Q}}{A\,F_D}\right\|^2}\right\}, \tag{147}$$

while the parameter a in Eq. (140) becomes

$$a = 1 - \left\|\frac{\underset{\sim}{Q}}{A\,F_D}\right\|^2 - \left(\frac{P^*}{B\,F_H}\right)^2 \tag{148}$$

If F_D goes to zero as σ tends to zero, as is the case with ISST soil if we disregard a very small cohesive strength, then it is possible for a to become negative, i.e.,

$$1 - \left\|\frac{\underset{\sim}{Q}}{A\,F_D}\right\|^2 - \left(\frac{P^*}{B\,F_H}\right)^2 < 0 \tag{149}$$

or

$$1 - \left\|\frac{\underset{\sim}{Q}}{A\,F_D}\right\|^2 < \left(\frac{P^*}{B\,F_H}\right)^2 \tag{150}$$

Thus, in view of Eq. (147), both roots of Δz will have the same sign. Furthermore, since $\Delta\sigma$ is negative during hydrostatic unloading, both roots will be positive and therefore inadmissible since one does not know which of the two positive roots is the correct one, i.e., there is a uniqueness problem.

5.2 SOURCE OF DIFFICULTY.

In order to determine whether or not the difficulty is of numerical origin, we took the following steps:

1. First, each of the problems was rerun with a variety of different size stress increments, which varied by over an order of magnitude. As an extreme case, we used 20,000 stress increments on the fourth leg alone. Regardless of the size of the stress increment, the computer program stopped (because of the condition $a < 0$) at virtually the same identical value of the hydrostatic pressure on the unloading leg in each case. The magnitude of the hydrostatic pressure at which this occurred was different, however, for each of the four cases considered. Thus, the difficulty did not appear to be due to increment size.

2. Secondly, we replaced the usual approach for obtaining the roots Δz of the quadratic equation (139) in the computer program by a more accurate approach. As most numericists are aware, if the usual expressions are used to determine the roots of a quadratic, serious difficulties can arise. In particular, if either a or c (or both) are small, then one of the roots will involve the subtraction of b from a very nearly equal quantity (the discriminant) and the root will be determined very inaccurately. The correct way to compute the roots is as follows. If we set

$$q \equiv -\frac{1}{2}\left[b + \mathrm{sgn}(b)\sqrt{b^2 - 4ac}\right], \tag{151}$$

then the two roots are

$$\Delta z_1 = \frac{q}{a} \quad \text{and} \quad \Delta z_2 = \frac{c}{q} \tag{152}$$

This method of determining the roots Δz_1 and Δz_2 was introduced into the computer program and had no perceptible effect on the results. The computer calculations continued to stop at the same locations on the hydrostatic unloading legs.

3. Next, the method of integrating the differential equations (119) to (121) for the Q_{*r}, P_i and N_i was improved. Consider, for example, the differential equation for Q_{*r} given by Eq. (119). A careful analysis shows that this differential equation can be integrated over a finite increment Δz to yield the following expression for the increment ΔQ_{*r}:

$$\Delta Q_{*r} = \left[\frac{1 - e^{-\alpha_r \Delta z_D}}{\alpha_r \Delta z_D}\right]\left[A_r \Delta \varepsilon_*^p - \alpha_r Q_{*r} \Delta z_D\right] \qquad (153)$$

where $\Delta z_D = \Delta z / F_D$. Similar expressions are obtained for ΔP_i and ΔN_i. Inasmuch as the term inside the first parentheses on the right side of this equation has the potential for numerical difficulties when Δz_D is small, we replaced this term with an accurate Padé approximation to avoid the difficulty. Again, the introduction of this improvement into the computer program had no perceptible effect on the calculational results and the calculations continued to stop at nearly the same location, as previously, on the hydrostatic unloading leg.

In view of the fact that none of the changes described above to the numerical scheme had any significant effect in alleviating the problem of the parameter a becoming negative on the hydrostatic unloading leg, it was concluded that the problem was not numerical in nature. Attention was then turned to the model itself.

We initially speculated that the problem may arise from the Dirichlet series representations for $\rho(z_D)$ and $\phi(z_H)$ and, to explore this, we developed approximate, but reasonable, representations of $\rho(z_D)$ and $\phi(z_H)$ based on the use of a single exponential in each case, which corresponds to one internal variable. Using these representations for $\rho(z_D)$ and $\phi(z_H)$, numerical studies of the problems of shear at constant pressure were redone, but this time the calculations proceeded to completion without difficulty over the entire four legs of the stress path. These results would certainly indicate that the difficulty was due to the Dirichlet series representations for $\rho(z_D)$ and $\phi(z_H)$. On further reflection, however, it was concluded that this is not realistic. Consider that a

Dirichlet series represents a solid of some kind and the only thermodynamic constraint is that the series consist of positive decaying exponential terms. If we accepted the above plausibility, one must conclude that some solids suffer from this difficulty and some do not, a conclusion which is physically unrealistic.

We now believe that the problem lies in the physics of the representation of the material behavior. For instance, in the developments to date, the parameters A_r have been assumed constant and the hardening function F_D has been taken to be a function of σ only, although there is strong evidence that it also depends on ϵ^p. To elaborate, we note that various soils with different initial porosities exhibit different responses to shear. Hence, porosity must affect F_D. However, since porosity and plastic volumetric strain ϵ^p are interrelated, plastic volumetric strain must also affect F_D. It is very likely that the same will be true of the parameters A_r. A study is needed to examine this dependence with a view toward ensuring that the parameter "a" in Eq. (140) is never negative, whatever the stress (or strain) path. This will ensure that the difficulty will not arise.

Section 6

CONCLUSIONS AND RECOMMENDATIONS

On the basis of the analysis described in the preceding sections of this report, the following conclusions and recommendations are given:

1. A new endochronic plasticity model for soils, which can describe both densification and dilatancy, has been successfully applied to laboratory data generated by WES for ISST soils.

2. Appropriate theoretical methods have been developed from which the material functions and parameters of the model can be evaluated directly from two types of soil tests, namely, (a) pure hydrostatic compression tests and (b) triaxial tests in which the soil is sheared at fixed hydrostatic (not confining) pressure.

3. An explicit, efficient numerical scheme was developed for numerically integrating the system of equations which govern the model. A corresponding computer program based on the numerical scheme was also developed and applied to several problems.

4. A difficulty with the governing equations arose when the computer program was applied to the case of shear at constant hydrostatic pressure. Specifically, on the final leg of the stress path for this case, which involves pure hydrostatic unloading, the computer program calculated inadmissible increments in the intrinsic time increment Δz.

5. A number of aspects of the numerical scheme were improved but none appeared to have any significant effect on alleviating the difficulty noted above. Decreasing the increment size by over an order of magnitude also had no noticeable effect. In view of this, it was concluded that the difficulty was not of numerical origin.

6. We believe that the difficulty lies in the physics of the representation of the material behavior. It appears that the mathematical representations adopted in the present model for some of the material functions may not be general enough to describe some of the observed behavior of soils. A study is needed to explore this issue, with the goal of ensuring that the difficulty noted above will not arise, whatever the stress or strain path.

In closing, we emphasize that this study represents the first attempt to apply the new endochronic plasticity model with dilatant capability to real soils and, in the course of the study, considerable new insight into the characteristics of the model was obtained. In view of the substantial promise shown by the model in describing the complex features of real soil behavior, we strongly recommend that a further study be undertaken to resolve the issue of the representation of material functions discussed above.

LIST OF REFERENCES

1. Valanis, K. C., "A Theory of Viscoplasticity Without a Yield Surface, Part I: General Theory", *Archs. Mechs.*, 23 (1971), 517.

2. Valanis, K. C., "Fundamental Consequences of a New Intrinsic Time Measure, Plasticity as a Limit of the Endochronic Theory", *Archs. Mechs.*, 32 (1980), 171.

3. Valanis, K. C., and H. E. Read, **Endochronic Plasticity**, 1988 (to be published).

4. Akers, S. A., U.S. Army Engineer, Waterways Experiment Station, Vicksburg, Mississippi, Private Communication, June 27, 1986.

5. Valanis, K. C., and H. E. Read, "An Endochronic Plasticity Theory for Concrete", *Mechs. of Matls.*, 5 (1986), 277.

6. Ehrgott, J. Q., "Calculation of Stress and Strain from Triaxial Test Data on Undrained Soil Specimens", U.S. Army Engineer, Waterways Experiment Station, Vicksburg, Mississippi, Miscellaneous Paper S-71-9, May 1971.

7. Clayton, C. R. I., and S. A. Khatrush, "A New Device for Measuring Local Axial Strains on Triaxial Specimens", *Geotechnique*, 36 (1986), 593.

8. Jardine, R. J., M. J. Symes and J. B. Burland, "The Measurement of Soil Stiffness in the Triaxial Apparatus", *Geotechnique*, 34 (1984), 323.

9. Valanis, K. C., "Endochronic Theory of Soils and Concrete", Proc. of Confr. on Constitutive Laws for Engineering Materials, Theory and Applications, Vol. 1, p. 247 (1987), edited by C. S. Desai *et al.*, Elsevier.

10. Valanis, K. C., and J. Peters, "A Constitutive Theory of Soils with Dilatant Capability", Report by ENDOCHRONICS, INC., to WES, (July 1987).

11. Valanis, K. C., "An Endochronic Plasticity Model for ISST Soils", A Report by ENDOCHRONICS, INC. to S-CUBED on the work performed under Subcontract P.O. No. 32937, (Feb. 1987).

12. Valanis, K. C., "Thermodynamics of Internal Variables in the Presence of Internal Forces", *J. App. Phys.*, 47, 4765 (1976).

13. Valanis, K. C., "Partial Integrability as a Basis for Existence of Entropy in Irreversible Systems", *ZAMM*, 63, 73 (1983).

14. Hildebrand, F. B., **Introduction to Numerical Analysis**, 2 Ed., McGraw-Hill, New York (1974).

15. Murakami, H., and H. E. Read, "A Second-Order Numerical Scheme for Integrating the Endochronic Plasticity Equations", submitted to *J. Computers and Structures* for possible publication, 1988.

16. Read, H. E., S-CUBED, La Jolla, CA., Internal Report, December 1987.

17. Valanis, K. C., and H. E. Read, "Endochronic Plasticity: Basic Equations and Applications", A Workshop presented at the 2nd International Congress and Short Course on Constitutive Laws for Engineering Matls: Theory and Application, Tucson, Arizona, January 1987.

Appendix A

TRANSFORMATION FROM ENGINEERING STRAIN TO NATURAL STRAIN

The ISST soil data recently supplied by WES to S-CUBED for model development are expressed in terms of engineering strains. Most of the materials models used in the defense community, however, are based upon the natural (or logarithmic) definition of strain. In developing a constitutive model from the WES data for eventual use in conjunction with one of the material response coeds, the engineering strains given in the data must be transformed to natural strains for consistency. The purpose of this appendix is to document the equations for making this transformation.

Analysis.

Consider the small element of material, shown in Figure 1, which has sides of length L_1^o, L_2^o, and L_3^o in the initial (unstrained) state.

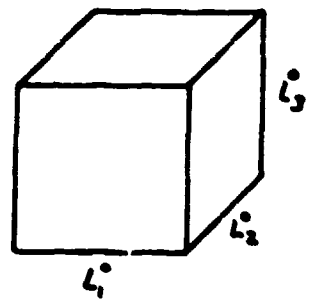

Figure 1. Unstrained configuration of material element.

The element is strained in (principal) directions perpendicular to its surfaces so that the lengths of the sides become L_1, L_2 and L_3. Under these conditions, the engineering strains, ϵ_i^E, can be expressed as

$$\epsilon_i^E = \frac{L_i - L_i^o}{L_i^o} \quad , \quad (i = 1,2,3) \tag{1}$$

while the corresponding natural strains, ϵ_i^N, are given by

$$\epsilon_i^N = - \int_{L_i^o}^{L_i} \frac{dL_i}{L_i} = \ell n\left(\frac{L_i}{L_i^o}\right) \qquad (i = 1,2,3) \tag{2}$$

The minus signs appear on the right-hand sides of Eqs. (1) and (2) so that the strains will be positive in compression, which is the sign convention commonly adopted in soil mechanics.

Equation (1) can be solved for L_i to give

$$L_i = L_i^o\left(1 - \epsilon_i^E\right) \qquad (i = 1,2,3) \tag{3}$$

which, when substituted into Eq. 2, leads to the expression

$$\boxed{\epsilon_i^N = - \ell n\left(1 - \epsilon_i^E\right)} \qquad (i = 1,2,3) \tag{4}$$

This equation, therefore, relates the engineering strains to the natural strains.

Let us consider now the volumetric strain. The engineering definition of volumetric strain is

$$\epsilon_v^E = - \frac{V - V_o}{V_o} \tag{5}$$

where V and v_o denote, respectively, the current and initial volumes of the element shown in Figure 1. In terms of natural strain, the volumetric strain is given by

$$\epsilon_V^N = - \int_{V_o}^{V} \frac{dV}{V} = - \ln\left[\frac{V}{V_o}\right] \tag{6}$$

In terms of the current and initial lengths of the sides of the small element, we can write

$$\frac{V}{V_o} = \frac{L_1 L_2 L_3}{L_1^o L_2^o L_3^o} \tag{7}$$

Equation (3) may be used in Eq. (7) to give

$$\frac{V}{V_o} = \left(1 - \epsilon_1^E\right)\left(1 - \epsilon_2^E\right)\left(1 - \epsilon_3^E\right) , \tag{8}$$

Combining this with Eqs. (5) and (6), we find

$$\epsilon_V^E = - \left[\left(1 - \epsilon_1^E\right)\left(1 - \epsilon_2^E\right)\left(1 - \epsilon_3^E\right) - 1\right] \tag{9}$$

and

$$\boxed{\epsilon_V^N = - \ln\left[\left(1 - \epsilon_1^E\right)\left(1 - \epsilon_2^E\right)\left(1 - \epsilon_3^E\right)\right]} \tag{10}$$

By setting

$$I_\epsilon = \epsilon_1^E + \epsilon_2^E + \epsilon_3^E$$

$$II_\epsilon = \epsilon_1^E\epsilon_2^E + \epsilon_2^E\epsilon_3^E + \epsilon_3^E\epsilon_1^E \qquad (11)$$

$$III_\epsilon = \epsilon_1^E\epsilon_2^E\epsilon_3^E \quad ,$$

Equations (9) and (10) can be re-expressed in the forms:

$$\epsilon_v^E = I_\epsilon - II_\epsilon + III_\epsilon \qquad (12)$$

$$\epsilon_v^N = -\ln(1 - I_\epsilon + II_\epsilon - III_\epsilon) \qquad (13)$$

For small strains, Eqs. (12) and (13) reduce to the usual expressions for the volumetric strain given by the infinitesimal theory, namely,

$$\epsilon_v^E = \epsilon_v^N = I_\epsilon \qquad (14)$$

Summary.

Equation (4) provides the transformation from axial engineering strains ϵ_i^E to natural strains ϵ_i^N, while Eq. (10) allows one to obtain the natural volumetric strain ϵ_v^N from the axial engineering strains, ϵ_i^E.

Appendix B

COMPUTER PROGRAM FOR ENDOCHRONIC SOIL MODEL, REQUIRING THE STRAIN HISTORY AS INPUT.

```
c     Index convention:
c
c           i = 1,...,numi
c           j = 1,...,numr
c           k = 1,...,3
c           l = 1,...,nleg(nl)
c           n = 1,...,SUM[nleg(nl)]
c           nl= 1,...,numleg
c
      parameter (maxi=10,maxl=13,maxr=10)
      implicit double precision (a-h,o-t)
      dimension de    ( 3 ) , dep   ( 3 ) , deps( 3 ) , ds  ( 3 ) ,
     .          e     ( 3 ) , ep    ( 3 ) , eps ( 3 ) , epso( 3 ) ,
     .          q     ( 3 ) , s     ( 3 ) , sig   ( 3 ) ,
     .          b     (maxi) , biggam(maxi) , beta(maxi) , bign(maxi) ,
     .          pi    (maxi) , smlgam(maxi) ,
     .          a     (maxr) , alpha (maxr) , qr(3,maxr) ,
     .          nleg  (maxl) , epsleg(3,maxl)
      character*60 ndfile,nofile
c
      read  210, nofile
      read  210, ndfile
      read    *, akzz ,am   ,amuz ,beth,bets,betk
      read    *, capkz,capk1,const,pr  ,taus,c0  ,sigt
      read    *, numr ,(a(j),alpha(j),                    j=1,numr)
      read    *, numi ,(b(i),beta (i),biggam(i),smlgam(i),i=1,numi)
      read    *, numleg,nleg(1),(epsleg(k,2),k=1,3)
c
      print 220, akzz ,am   ,amuz ,beth,bets,betk
      print 230, capkz,capk1,const,pr  ,taus,c0  ,sigt
      print 240, (j,a     (j),j,alpha (j),j=1,numr)
      print 250, (i,b     (i),i,beta  (i),i=1,numi)
      print 260, (i,biggam(i),i,smlgam(i),i=1,numi)
      print 270, (1,nleg(1),(epsleg(k,1+1),k=1,3),l=1,1)
c
      open(unit=11,file=ndfile,form='formatted')
      open(unit=12,file=nofile,form='formatted')
      read (11,*)
      read (11,*)
      read (11,*)
      read (11,*)
      read (11,*)
      read (11,*)
      read (11,*)
      read (11,*)
      read (11,*)
c
      write (12,310)
c
      capa=0.
      do 10 j=1,numr
   10 capa=capa+a(j)
c
      capb=0.
      gam0=0.
      do 20 i=1,numi
```

```
      capb=capb+b(i)
   20 gam0=gam0+biggam(i)
c
      n=1
c
      do 120 nl=1,numleg
c
      epold1=epnew1
      epold2=epnew2
      epold3=epnew3
      read (11,*)   epnew1,epnew2,epnew3
      epnew1=-epnew1
      epnew2=-epnew2
      epnew3=-epnew3
c
      do 110 nn=1,nleg(1)
c
      nsteps=n
      n     =n+1
      epso(1)=eps(1)
      epso(2)=eps(2)
      epso(3)=eps(3)
      eps (1)=epold1+(epnew1-epold1)*(float(nn))/float(nleg(1))
      eps (2)=epold2+(epnew2-epold2)*(float(nn))/float(nleg(1))
      eps (3)=epold3+(epnew3-epold3)*(float(nn))/float(nleg(1))
c
      dev=0.
      do 40 k=1,3
      deps(k)=eps(k)-epso(k)
   40 dev=dev+deps(k)
      ev =ev +dev
c
      do 60 k=1,3
      q(k)=0.
      do 50 j=1,numr
   50 q (k)=q   (k)+alpha(j)*qr(k,j)
      e (k)=eps (k)- ev/3.
   60 de(k)=deps(k)-dev/3.
c
      p =0.
      fn=0.
      do 70 i=1,numi
      fn=fn+smlgam(i)*bign(i)
   70 p =p+beta(i)*pi(i)
c
      qde =0.
      qq  =0.
      qs  =0.
      sde =0.
      dede=0.
      do 80 k=1,3
      qde =qde +q (k)*de(k)
      qq  =qq  +q (k)*q (k)
      qs  =qs  +s (k)*q (k)
      sde =sde +s (k)*de(k)
   80 dede=dede+de(k)*de(k)
```

```
c
      akz =akzz*dexp(-betk*evp)
      capk=capkz+capk1*pp
      amu2=amuz+const*dsqrt(gamz)
      gam =gam0*exp(-c0*evp)
      fs  =(taus+beta*pp)/(taus+beta*pr)
      fh  =dexp(beth*evp)
c
      abar=capa*amu2
      bbar=capb+capk
      sma=1.-qq/(abar*fs)**2
     .    -(1./bbar**2)*((p+fn)/fh-akz*gam*qs/(abar*fs))**2
      smb=-2*(amu2*qde/(abar**2*fs)+(akz/bbar)**2
     .    *(capk*dev-gam*amu2/abar*sde)*((p+fn)/(akz*fh)
     .    -gam*qs/(abar*fs)))
      smc=-((amu2/abar)**2*dede+(akz/bbar)**2*(capk*dev
     .    - amu2*gam*sde/abar)**2)
      arg =smb**2-4.*sma*smc
      dz1 =-(.5/sma)*(smb+dsign(1.d0,smb)*dsqrt(max(0.,arg)))
      dz2 =smc/(sma*dz1)
      if (arg.lt.0..or.dz1*dz2.gt.0.) then
           print 290, nl,nsteps,arg,dz1,dz2
           end if
      dz =max(dz1,dz2)
      dzs=dz/fs
      dzh=dz/(akz*fh)
c
      devp=(1./bbar)*(capk*dev-amu2*gam
     .       /abar*sde+((p+fn)/(akz*fh)-gam*qs/(abar*fs))*dz)
      evp =evp+devp
      dwp =0.
      do 90 k=1,3
      dep(k)=(amu2*de(k)+q(k)*dz/fs)/abar
      ep (k)=ep(k)+dep(k)
      ds (k)=capa*dep(k)-q(k)*dz/fs
      s  (k)=s(k)+ds(k)
      dwp   =dwp+s(k)*dep(k)
      do 90 j=1,numr
      ems1=dexp  (-alpha(j)*dzs)
      ems2=dxp1dx( alpha(j)*dzs)
      ems =ems1*ems2
   90 qr(k,j)=qr(k,j)+ems*(a(j)*dep(k)-alpha(j)*qr(k,j)*dzs)
      pp=pp+capb*devp+gam*dwp-((p+fn)/(akz*fh))*dz
      do 925 k=1,3
  925 sig(k)=s(k)+pp
c
      do 100 i=1,numi
      bign(i)=bign(i)+gam0*exp(-c0*evp)*dwp
     .       -bign(i)*smgam(i)*dz/(akz*fh)
      emh=dexp(-beta(i)*dzh)*dxp1dx(beta(i)*dzh)
  100 pi(i)=pi(i)+emh*(b(i)*devp-beta(i)*pi(i)*dzh)
      gamz =dsqrt((eps(1)-eps(2))**2
     .     +      (eps(2)-eps(3))**2
     .     +      (eps(3)-eps(1))**2)/3.
      if (sig(1).le.sigt.or.sig(2).le.sigt.or.sig(3).le.sigt) go to 130
c
```

```
      write (12,320) n,(eps(k),k=1,3),(sig(k),k=1,3)
c
  110 continue
c
  120 continue
c
  130 call exit
c
  210 format(a)
  220 format(    ' akzz   =',1pe13.6,   '    am     =',1pe13.6,
     .       ,   amuz   =',1pe13.6,/,
     .           ' beth   =',1pe13.6,   '    bets   =',1pe13.6,
     .         ,   betk   =',1pe13.6)
  230 format(    ' capkz  =',1pe13.6,   '    capk1  =',1pe13.6,
     .       ,   const  =',1pe13.6,/,
     .           ' pr     =',1pe13.6,   '    tauz   =',1pe13.6,
     .           ' c0     =',1pe13.6,   '    sigt   =',1pe13.6)
  240 format(/,(' a',i1,'     =',1pe13.6,'    alpha',i1,' =',1pe13.6))
  250 format(/,(' b',i1,'     =',1pe13.6,'    beta',i1,'  =',1pe13.6))
  260 format(  (' biggam',i1,'=',1pe13.6,'    smlgam',i1,'=',1pe13.6))
  270 format(/,(' leg',i2,',',i6,' points,   sigleg =',1p3e14.6))
  280 format('nsteps =',i5)
  290 format('nl,nsteps,arg,dz1,dz2',2i6,1p3e15.7)
  310 format(' strain drive endochronic model results',/,
     .       ,          e1         e2         e3     ',
     .             '    sig1       sig2       sig3   ')
  320 format(i5,3f10.6,3f10.4)
c
      end
```

DISTRIBUTION LIST

DEPARTMENT OF DEFENSE

Director
Defense Nuclear Agency
ATTN: DFSP (Dr. G. W. Ullrich)
SPWE (Mr. C. B. McFarland)
SPWE (MAJ Mike Pelkey)
SPWE (Dr. E. J. Rinehart)
Technical Library
Washington, DC 20305-1000

Director
Defense Nuclear Agency
Nevada Operations Office
ATTN: TDNV (Mr. J. W. LaComb)
P.O. Box 98518
Las Vegas, NV 89193-8518

Director
Defense Advanced Research Project Agency
ATTN: Technical Library
1400 Wilson Blvd.
Arlington, VA 22209

Director
Defense Intelligence Agency
ATTN: Technical Library
Washington, DC 20301-6111

Defense Technical Information Center
ATTN: TC
Cameron Station
Alexandria, VA 22314

DEPARTMENT OF THE ARMY

Commander
US Army Corps of Engineers
ATTN: CERD-L
CERD-M (Mr. B. O. Benn)
CEEC-ET (Mr. R. L. Wight)
CEIM-SL
Washington, DC 20314-1000

Division Engineer
US Army Engineer Division, Huntsville
ATTN: CEHND-SR
P.O. Box 1600
Huntsville, AL 35807-4301

Director
US Army Construction Engineering Research Laboratory
ATTN: Technical Library
P.O. Box 4005
Champaign, IL 61820-1305

District Engineer
US Army Engineer District, Omaha
ATTN: CEMRO-ED-S (Mr. Bob Kelley)
CEMRO-ED-SH (Mr. Bill Gaube)
215 N. 17th Street
Omaha, NE 61802-4978

Commander/Director
US Army Cold Regions Research and Engineering Laboratory
ATTN: Technical Library
72 Lyme Road
Hanover, NH 03755-1290

DEPARTMENT OF THE ARMY (CONTINUED)

Commandant
US Army Engineer School
ATTN: ATZA-CD (COL Fred Parker)
Technical Library
Fort Belvoir, VA 22060-5281

Commander
Harry Diamond Laboratories
Department of the Army
ATTN: Technical Library
2800 Powder Mill Road
Adelphi, MD 20783-1197

Commander
US Army Nuclear and Chemical Agency
ATTN: Technical Library
7500 Backlick Road, Bldg. 2073
Springfield, VA 22150

DEPARTMENT OF THE NAVY

Naval Civil Engineering Laboratory
ATTN: Technical Library
Port Hueneme, CA 93043

Naval Facilities Engineering Command
200 Stoval Street
ATTN: Technical Library
Alexandria, VA 22332

DEPARTMENT OF THE AIR FORCE

Air Force Institute of Technology
Air University
ATTN: Technical Library
Wright-Patterson AFB, OH 45433

Air Force Office of Scientific Research
ATTN: Technical Library
Bolling AFB, DC 20332

Air Force Weapons Laboratory (AFSC)
ATTN: Technical Library
Kirtland AFB, NM 87117-6008

Air Force Engineering and Services Center (AFSC)
ATTN: Technical Library
Tyndall AFB, FL 32403

Commander
Ballistic Missile Office (AFSC)
ATTN: MYEB (LTC D. H. Gage)
Technical Library
Norton AFB, CA 92409-6468

DEPARTMENT OF ENERGY

Lawrence Livermore National Laboratory
ATTN: Technical Library
P.O. Box 808
Livermore, CA 94550

Los Alamos National Laboratory
ATTN: Technical Library
P.O. Box 1663
Los Alamos, NM 87545

DEPARTMENT OF ENERGY (CONTINUED)

Sandia National Laboratories
ATTN: Technical Library
P.O. Box 5800
Albuquerque, NM 87185

Sandia National Laboratories
ATTN: Technical Library
Livermore, CA 94550

DEPARTMENT OF DEFENSE CONTRACTORS

Mr. J. L. Bratton
Applied Research Associates, Inc.
4300 San Mateo Blvd., NE, Suite A220
Albuquerque, NM 87110

Mr. S. E. Blouin
Applied Research Associates, Inc.
Box 120A, Waterman Road
South Royalton, VT 05068

Mr. J. L. Drake
Applied Research Associates, Inc.
3202 Wisconsin Avenue
Vicksburg, MS 39180

Dr. J. G. Trulio
Applied Theory, Inc.
930 S. LaBrea Avenue
Los Angeles, CA 90036

Dr. Y. Marvin Ito
Mr. S. H. Schuster
California Research & Technology, Inc.
20943 Devonshire Street
Chatsworth, CA 91311-2376

Dr. Hon-Yim Ko
Department of Civil, Environmental, and
Architectural Engineering
University of Colorado at Boulder
Boulder, CO 80309

Dr. K. C. Valanis (10 copies)
Endochronics, Inc.
8605 Northwest Lakecrest Court
Vancouver, WA 98665

New Mexico Engineering Research Institute
ATTN: Technical Library
University of New Mexico
Box 25, University Station
Albuquerque, NM 87131

Dr. Don Simons
Dr. M. M. Balaban
R&D Associates
P.O. Box 9695
Marina del Rey, CA 90291

Dr. H. E. Read (10 copies)
Mr. Steve Peyton
Mr. Norton Rimer
S-Cubed
P.O. Box 1620
La Jolla, CA 92038-1620

DEPARTMENT OF DEFENSE CONTRACTORS (CONTINUED)

Dr. A. L. Florence
Dr. Lynn Seaman
SRI International
333 Ravenswood Avenue
Menlo Park, CA 94025

Mr. S. J. Green
Terra Tek, Inc.
420 Wakara Way
Salt Lake City, UT 84108

Mr. Norman Lipner
Dr. M. G. Katona
TRW Defense Systems Group
P.O. Box 1310
San Bernardino, CA 92402

Dr. D. J. Mess
TRW Defense and Space Systems Group
One Space Park, Bldg. 134/Rm 9835
Redondo Beach, CA 90278

Dr. I. S. Sandler
Weidlinger Associates
333 Seventh Avenue
New York, NY 10001

Dr. Jeremy Isenberg
Weidlinger Associates
620 Hansen Way, Suite 100
Palo Alto, CA 94304

Dr. W. F. Carroll
Department of Civil Engineering
and Environmental Sciences
University of Central Florida
Orlando, FL 32816

Dr. R. T. Allen
Dr. Dan Patch
Science Applications International Corp.
Pacifica Technology Division
P.O. Box 148
Del Mar, CA 92014